Span Sensitivity of the Scripps Interferometric Oxygen Analyzer

Ralph F. Keeling

Stephen J. Walker

William Paplawsky

Scripps Institution of Oceanography

UC San Diego

December, 2020

Table of Contents

1. Overview

Since program inception, the Scripps O_2 program has carried out measurements of changes in atmospheric O_2 abundance using an interferometric method, as described in Chapter 2 of Keeling (1988a) and in Keeling et al (1998). This report provides an overview of the factors influencing the span sensitivity of the interferometer in support of an update to the span sensitivity implemented in Aug. 2017. The report also provides an estimate of the residual uncertainty in the span calibration factor, following this correction.

The 2017 span update has been retrospectively applied to all O_2/N_2 measurements from the interferometer, back to 1989, and is implemented in database versions starting with the 10 Aug 2017 archive. The reprocessing involved new determinations of calibration tanks and propagating these forward starting from program inception. This new scale is called the SIO2017 O_2/N_2 scale. The update has implications for reference gas calibrations performed at Scripps for other groups, and it has implications for publications using prior versions of the data, particularly those relying on long-term trends in O_2/N_2, such as those reporting global land and ocean carbon sinks (e.g. Manning and Keeling, 2006, Keeling and Manning, 2014). The update has the effect of increasing by the global ocean carbon sink estimated by the O_2 method by approximately 0.16 Pg C yr^{-1}. The land sink decreases by an equal amount. The recent application of the O_2/N_2 data to estimate ocean heat uptake (Resplandy et al., 2019), used a version from after the update, but also used a preliminary estimate of the span uncertainty of ±2%. This report indicates that errors in span (after the update) are likely not higher than ±1%. The relationship between new and old values of O_2/N_2 ratio are shown in Figure 1.

This report describes methods and results that may have relevance beyond the context of the span update. Section 2 reviews the theoretical basis for the interferometric method, including details and formalism such as interference factors for Ar/N_2, not presented previously. Section 4 describes a diagnostic method involving bleeding an O_2/CO_2 mixture into air, presented previously only in Ph.D. theses (Severinghaus, 1995, Blaine, 2005). Section 5 describes methods and results from gravimetric standards prepared by R. Keeling in 1992 but not previously described, which have relevance not just for span sensitivity but for the absolute anchoring of the Scripps O_2/N_2 scale. Section 6 describes new tests to quantify the magnitude of any incomplete sample/reference sweep-out on the span sensitivity, also documenting a method implemented since Nov. 2002 to validate sweep-out curves for flasks using multiple working tanks.

The interferometeric method determines changes in O_2/N_2 ratio based on the relative (temporal) position of interference fringes generated in a two-wavelength interferometer. In effect, the fringes at one wavelength (2537.2688Å) are used as a metric for assessing the position of fringes at the other wavelength (4359.5662Å). Changes in the O_2/N_2 ratio of air in the sample cell lead to changes in the refractivity ratio, which in turn changes the relative fringe positions. The span sensitivity is generally reported in per meg units per ten thousandths of a fringe.

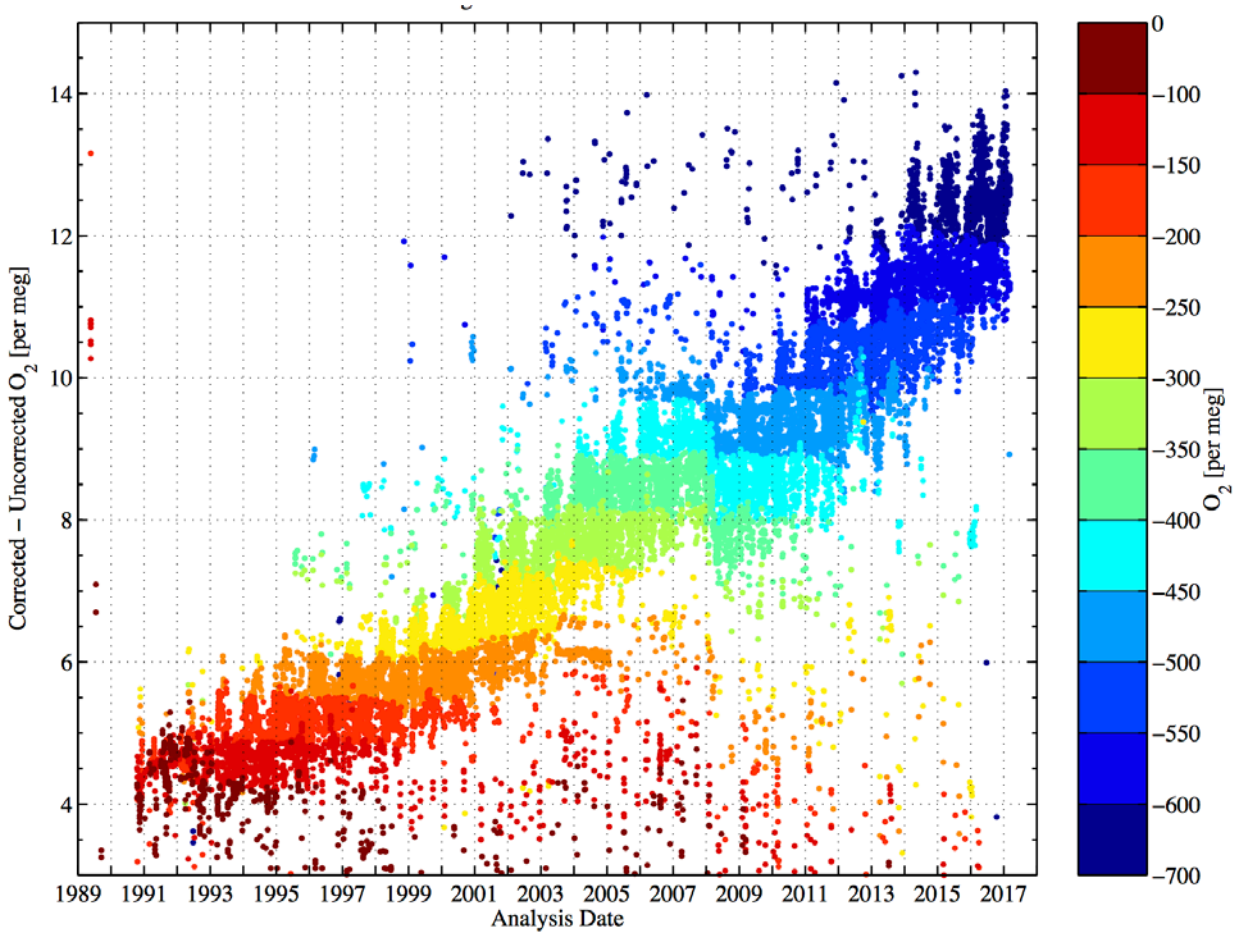

Figure 1. Adjustments applied to the O_2/N_2 ratio for all flasks and cylinders measured on the interferometer. The colorbar indicates the O_2/N_2 ratio of the flask or cylinder prior to adjustment, and the y-value is the adjustment applied in the correction.

This report makes use of three independent controls on the span sensitivity of the interferometer. The first control is theoretical, and depends on the refractivities of air and pure O_2, and on the optical path difference (OPD) of the interferometer. The OPD has been measured periodically by counting fringes as the interferometer sample cell is filled from vacuum. The second control is based on bleeding a small controlled amount of a gravimetrically prepared O_2:CO_2 mixture into the air stream passing through the interferometer. In this "bleed test" method, the change in CO_2 concentration, measured using a calibrated infrared analyzer, is used to assess the actual change in O_2/N_2 ratio which can be compared against the interferometer measurement. The third control is based on a suite of six gravimetrically-prepared air-like mixtures prepared in 1992, with known O_2/N_2 ratios, which span a range of several thousand per meg in O_2/N_2 around ambient air values. Data reduction has always depended on the theoretical span relationship, with the other methods applied as cross checks.

A review of procedures around 2015 motivated several changes which this report addresses. The first and most significant change is correcting a transcription error in one of the

coefficients used for the theoretical span sensitivity. By itself, this error caused O_2/N_2 differences to be overreported by 2.2%. The second change involves adopting new procedures for calculating the optical path differences of the interferometer, taking information on pressure gage performance and lab temperature more fully into account. An additional very minor change is using a new estimate of the absolute O_2 mole fraction based on gravimetric results reported in this report.

The data reduction procedures for the interferometer allow for a different value of the theoretical span sensitivity on each analysis date, inferred from daily changes in OPD tied to pressure as recorded via an electronic pressure gage (10000 Torr MKS Baratron). The changes supported by this report therefore provide a new estimated span sensitivity for each analysis date.

The essential result is summarized in Figure 2, which shows the span correction factor, i.e. the ratio of the new to old theoretical span sensitivity, as a function of time since program inception in 1989. The two main changes to the theoretical span sensitivity, i.e. from the transcription error and the revised daily estimates of the OPD, tend to partly compensate, especially in the early years (1989-1992). Bleed tests to check the span were carried out in 1994, 2001, and three times in 2015. Runs of the gravimetric tanks were carried out in 1992, 1993, 2012, and 2015. As shown in Figure 2, these cross checks strongly support the changes based on the theoretical considerations, with all three methods agreeing to within ~1%.

This report suggests that a major source of residual uncertainty in the theoretical span sensitivity, after this update, arises from the limited accuracy in the determinations of the OPD, ultimately tied to uncertainty in the temperature of the main cell block of the interferometer and the pressure in the sample cell of the interferometer. The other factors involved in the theoretical span sensitivity depend on gas refractivity data and composition of the reference gas, which are accurately-known fixed constants. Their uncertainty contributes to less than 0.1% uncertainty in span sensitivity. The true span sensitivity may differ from the theoretical sensitivity due to incomplete sample/reference sweep-out, which would cause differences to be underreported. Currently no correction is applied for incomplete sweep-out. Bounds on the magnitude of any such effect are discussed Section 6.

This report provides evidence that a small span error may persist in the Scripps scale, such that differences in O_2/N_2 are underreported by an amount less than 1%. The comparison from gravimetric tanks suggest an O_2/N_2 correction of $0.6 \pm 0.8\%$. Tests aimed at assessing scale contraction due to incomplete sweep-out suggest an effect of $\sim 0.5 \pm 0.5\%$. A sweep-out effect is a possible explanation, but other errors may contribute, such as inaccuracies in the OPD. The effect is also within the noise of the determinations.

The report motivates several possible improvements to reduce uncertainties. The impact of incomplete sample/reference sweep-out could be better assessed repeating the procedures but with using tanks with larger differences in O_2/N_2. This incomplete sweep-out correction is expected to be very stable in time, so could be applied retrospectively. The OPD determinations

could easily be improved in the future through upgrades in the temperature and pressure measurements. By calibrating these against absolute fringe count on filling the cell, it should be possible to establish the OPD to the 10^{-4} level. Ultimately, a stable span calibration to the level of 0.1% seems feasible.

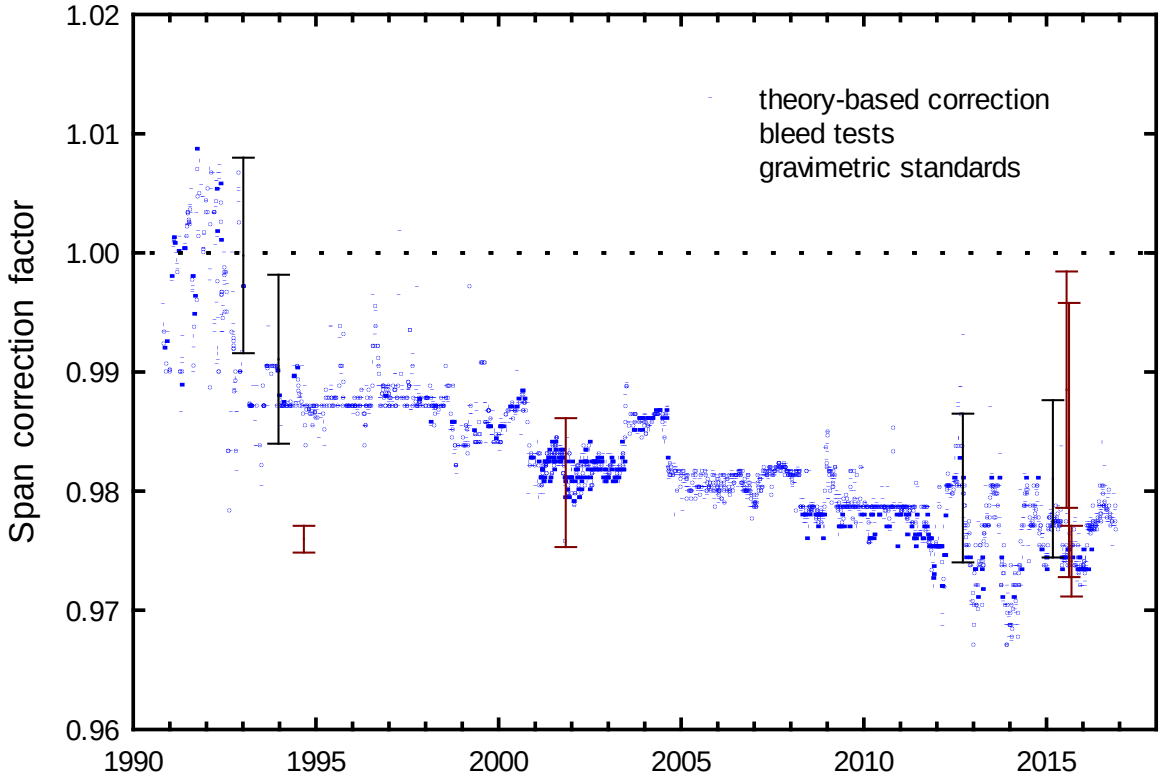

Figure 2. Comparison of span calibration factor used for interferometric measurements before and after changes implement through this report. A span correction factor of 0.98 implies that a previously-reported difference of 100 per meg (on a particular date) should actually have been 98 per meg. The theory-based correction uses revised estimates of the refractivity ratio sensitivity coefficient (Table 2) and revised estimates of the optical path difference, $OPD_{samp}(\lambda_2)$. The bleed tests are based on adding a small amount of a known O_2;CO_2 mixture into an air stream, and using the manometrically-calibrated CO_2 measurement to assess the change in O_2/N_2. The gravimetric standard comparison was based on measuring a suite of six gravimetrically prepared air-like mixtures, which spanned a range in O_2/N_2 ratio. The gravimetric results are based on analysis prior to the update in span sensitivity (Table 9 results below are after update).

2. Theoretical Span Sensitivity

The interferometric method depends on relating changes in O_2 abundance to changes in the refractivity of air between two emissions lines of a ^{198}Hg electrodeless discharge lamp, at vacuum wavelengths λ_1 = 2537.2688Å and λ_2 = 4359.5662Å (Kaufman, 1962). The refractivity ratio or "relative refractivity" of a sample is defined according to

$$\tilde{r} = \frac{n(\lambda_1)-1}{n(\lambda_2)-1} \quad (1)$$

where n(λ)-1 is the refractivity at wavelength λ. While the refractivity of a dilute gas increases roughly linearly with pressure, the refractivity ratio, in contrast, is largely independent of pressure, depending only on composition. For small deviations from a reference, Keeling (1988a, Appendix A) showed that,

$$\delta\tilde{r} = S_i \delta X_i \quad (2)$$

where δX_i is the change in mole fraction of species *i* and where S_i is a constant sensitivity coefficient given by

$$S_i = \frac{n_i(\lambda_2)-1}{n_{air}(\lambda_2)-1} \cdot \frac{\tilde{r}_i(\lambda_1,\lambda_2)-\tilde{r}_{air}(\lambda_1,\lambda_2)}{1-X_i} \quad (3)$$

where the quantities for air in Eq. (3) are evaluated at the concentration of the reference. Eq. (3) is valid as a single species *i* is added to or removed and as relative abundances of all other species are kept fixed. Eq. (2) is a linear approximation, valid for small deviations from the reference. The derivation of Eq. (3) rests only on the assumption that the refractivity of a gas mixture is equal to the sum of the refractivities of the constituents, which holds for dilute mixtures (Keeling, 1988a).

In order to generalize Eq. (2) to apply to changes involving multiple species, it is convenient to shift to a basis which expresses each species relative to N_2, e.g.

$$\delta(O_2/N_2) = \frac{(O_2/N_2)_{sample}}{(O_2/N_2)_{reference}} - 1 \quad (4)$$

where $\delta(O_2/N_2)$ is conventionally multiplied by 10^6 and expressed in "permeg" units. The change in O_2/N_2 in delta notation can be related to the change in the O_2 mole fraction relative to the reference according to

$$\delta(O_2/N_2) = \frac{\delta X_{O2}}{X_{O2}(1-X_{O2})} \quad (5)$$

where X_{O2} is the O_2 mole fraction of the air reference. Eq. (5) is valid in parallel with Eq. (2) when O_2 is added to or removed from air for small changes, although it is not valid under all manipulations (e.g. addition of CO_2). Relationships similar to Eq. (4) and (5) can also be written for Ar, CO_2, etc., using $\delta(Ar/N_2)$, $\delta(CO_2/N_2)$ etc. A generalized extension of Eq. (2) can then be written

$$\delta\tilde{r}_{samp} = \sum_{i \neq N_2} S_i X_i (1 - X_i)\, \delta(i/N_2) \qquad (6)$$

The sum in Eq. (6) is taken over all species other than N_2. Eq. (6) is an exact relationship, valid for small deviations from the reference. (In contrast, an extension of Eq. (2) involving a sum over terms involving mole fraction changes would not be exact because of cross influences, e.g. addition or removal of O_2 from a sample would impact not just the O_2 term, but also all other terms via the diluting effect of O_2 on the mole fraction of other species.).

Eq. (6) is valid, not just for manipulations involving O_2, Ar, CO_2, etc., but also for manipulations involving N_2. This is clear because adding N_2 is equivalent to removing all other gases simultaneously in proportion to their reference abundances, at least in terms of the effect on $\delta(i/N_2)$. Eq. (6) is valid for all these gases separately, so it must also be valid for this proportional manipulation. That Eq. (6) is valid for N_2 can also be shown by starting with an equation analogous to Eq. (6), but with N_2 replaced with an alternate reference species, such as Ar. This leads to an equation identical to Eq. (6) but with Ar replacing N_2 and vice versa in every instance (e.g. replacing $\delta(O_2/N_2)$ with $\delta(O_2/Ar)$, S_{Ar} with S_{N2}, etc.). This alternate equation can be shown to be identical to Eq. (6) using $\delta(O_2/Ar) = \delta(O_2/N_2) - \delta(Ar/N_2)$ and $\delta(N_2/Ar) = -\delta(Ar/N_2)$ and the definition (Keeling, 1988, Appendix A) of n_{air} and r_{air} in terms of constituent contributions. To calculate changes in $\delta\tilde{r}_{samp}$ for manipulations involving N_2, it may nevertheless be more straightforward to use Eq. (3) than Eq. (6). The relative sensitivity of the refractivity ratio to N_2 versus O_2 is also addressed in Appendix A below.

For atmospheric measurements, it is convenient to recast Eq. (6) as follows:

$$\delta\tilde{r}_{samp} = S_{O2} \cdot X_{O2}(1 - X_{O2})\delta(O_2/N_2) + S_{Ar} \cdot X_{Ar}(1 - X_{Ar}) \cdot \delta(Ar/N_2) + S_{CO2} \cdot \delta X_{CO2} + \ldots \qquad (7)$$

where additional trace gases can be handled analogously to CO_2. Eq. (7) approximates $\delta(CO_2/N_2)(X_{CO2})(1 - X_{CO2}) \approx \delta X_{CO2}$, etc., which is valid to a high level for changes in air. (This approximation neglects very small dilution effects, such as the reduction in X_{CO2} that results from O_2 addition).

It is also convenient to express the sensitivity of the refractivity ratio to changes in trace gases using interference factors I_i where

$$I_i = \frac{S_i / S_{O2}}{X_{O2}(1 - X_{O2})} \qquad (8)$$

which has units of permeg $\delta(O_2/N_2)$ per ppm of the trace gas. The sensitivity of the refractivity ratio to changes in $\delta(Ar/N_2)$ can also be expressed with an interference factor

$$I_{Ar/N2} = \frac{S_{Ar} X_{Ar}(1 - X_{Ar})}{S_{O2} X_{O2}(1 - X_{O2})} \qquad (9)$$

which has units of permeg/permeg.

Mole fractions in Eq. (1) through (9) are defined on a H_2O-free basis. This basis is appropriate because the procedures used on the interferometric O_2 analyzer involve drying sample and reference gases at the point of collection/pumping, with further drying of samples and reference gases to a uniform low level using a ~−90 °C cold trap immediately upstream of the interferometer.

Changes in refractivity ratio are measured using the two-arm interferometer described in Keeling (1988). The interferometer has one gas cell on each arm, i.e. a "sample cell" and a "scanning cell". The overall optical path difference of the interferometer includes contributions from both sample and scanning cell

$$OPD(\lambda) = OPD_{samp}(\lambda) - OPD_{scan}(\lambda) \tag{10}$$

where the *samp* subscript refers to the gas in the sample cell, which may alternately be filled with samples or reference gases. The refractivity ratio of the gas in the sample cell is related to OPD_{samp} according to

$$\tilde{r}_{samp} = \frac{\lambda_2}{\lambda_1}\frac{OPD_{samp}(\lambda_1)}{OPD_{samp}(\lambda_2)} \tag{11}$$

A similar equation holds for $\tilde{r}_{scan}$, the refractivity ratio of the gas in the scanning cell. The scanning cell is used only to modulate the optical path difference and create temporal fringes for analysis. The fringes are modulated by repeatedly bleeding in air from a "scan tank", and re-evacuating. The scan tank contains compressed natural background air. The analysis resolves changes in optical path difference $OPD(\lambda_1)$ at a fixed optical path difference $OPD(\lambda_2) = p_2$, where p_2 is an exact integer fringe order. The change in $OPD(\lambda_1)$ can be expressed in terms of the fringe remainder ε_1, defined according to $OPD(\lambda_1) = p_1 + \varepsilon_1$ where p_1 is also an exact integral fringe order. The fringe remainder ε_1 is related to the $\tilde{r}_{samp}$ according to

$$p_1 + \varepsilon_1 = \frac{\lambda_2}{\lambda_1}(\tilde{r}_{samp} - \tilde{r}_{scan})OPD_{samp}(\lambda_2) + \frac{\lambda_2}{\lambda_1}\tilde{r}_{scan}p_2 \tag{12}$$

Eq. (11) and (12) are identical to Eqs. 2.9 and 2.18 in Keeling (1988) except for neglecting fixed contributions to optical path differences that are unrelated to the gas composition, such as due to imperfections in the optics. Differentiating Eq. (12) to isolate the sensitivity of ε_1 to changes in $\tilde{r}_{samp}$ yields

$$\delta\varepsilon_1 = \frac{\lambda_2}{\lambda_1}OPD_{samp}(\lambda_2)\delta\tilde{r}_{samp} \tag{13}$$

Solving Eq. (7) for $\delta(O_2/N_2)$ yields

$$\delta(O_2 / N_2) = \frac{1}{S_{O2}} \cdot \frac{1}{X_{O2}(1 - X_{O2})} \cdot \delta\tilde{r}_{samp} + \; interference\, terms \tag{14}$$

which when combined with (13) yields the overall sensitivity relation

$$\delta(O_2 / N_2) = O2Span \cdot \delta\varepsilon_1 + \; interference\, terms \tag{15}$$

where

$$O2Span = \frac{\lambda_1}{\lambda_2} \cdot \frac{1}{OPD_{samp}(\lambda_2)\, S_{O2}} \cdot \frac{1}{X_{O2}(1 - X_{O2})} \tag{16}$$

Eq. (16) gives the theoretical span sensitivity of the interferometer, which depends on Hg lamp wavelengths, λ_1 and λ_2, on the optical path difference $OPD_{samp}(\lambda_2)$, the refractivity ratio sensitivity coefficient S_{O2}, and the absolute O_2 mole fraction in the air reference, X_{O2}. These parameters are all effectively time-invariant constants with the exception of $OPD_{samp}(\lambda_2)$, which depends and the sample cell length and the density of air in the cell, which in principle can vary from day to day. At a typical cell pressure of 1750 torr, corresponding to $OPD_{samp}(\lambda_2) \approx 3780$, Eq. (16) yields *O2Span* = 26400 per meg per fringe or 2.64 per meg per ten thousandths of a fringe.

To account for interferences, we routinely correct for changes in CO_2 using the interference factor from Eq. (8), but we neglect contributions from other trace gases, which have much smaller interferences. CO_2 is measured in samples and references using a Siemens non-dispersive infrared (NDIR) analyzer. On tropospheric air samples, the interference from changes in Ar/N_2 ratio is negligible because the Ar/N_2 interference factor is very small ($I_{Ar/N2} \sim -0.012$ permeg/permeg) and because changes in $\delta(Ar/N_2)$ are typically at least four times smaller than those for $\delta(O_2/N_2)$.

Eq. (12) indicates that the fringe remainder is potentially sensitive to sample composition, not just via $\tilde{r}_{samp}$, but also via $OPD_{samp}(\lambda_2)$, which depends on the absolute refractivity of the sample and therefore also depends on the O_2/N_2 ratio of the sample. The former contribution, which is the main contribution, is isolated in Eq. (13). The latter contribution is addressed in Appendix B, where it is shown to be more than 10,000 times smaller.

3. Parameters for theoretical sensitivity relation

Refractivity ratio sensitivity coefficients

Table 1 summarizes the constants needed to calculate the sensitivity coefficients for the refractivity ratio of air, via Eq. (3), to changes in the relative abundance of the different gases. Table 1 updates the estimate for S_{O2} relative to Keeling et al. (1998), correcting an error in the calculation which can be traced to a transcription error in the relevant lab notebook (Interferometer Labbook #7, pages 76 and 110). The new estimate is higher than the Keeling (1998) value by 2.2%. The revised S_{O2} value incorporates a revised estimate for X_{O2} and incorporates small updates to the refractivity data, which cause changes of order 0.02%.

Table 1.

	Mole fraction, μmol mol^{-1} [a]	Refractivity ratio, $\tilde{r}_i$ from 4359.57 to 2537.27 Å	Refractivity at 0 °C, 760 torr, at 4359.57 Å × 10^4 [c]	Sensitivity coefficient, $S_i \times 10^8$, ppm^{-1}	Interference factor[d], I_i	Sensitivity coefficients from Keeling et al. (1998)
Dry Air		1.069006[b]	2.965			
N_2	780840	1.062024[b]	3.023	-3.2479		
O_2	209448	1.097922[b]	2.754	3.3973		3.320
Ar	9333.5	1.061265[b]	2.854	− 0.7521	− 0.0124	
CO_2	363.29	1.073000[b]	4.562	0.6147	1.0928	0.614
Ne	18.2	1.0244[c]	0.6754	-1.016	-1.806	
He	5.2	1.0250[c]	0.3511	-0.521	-0.926	
Kr	1.1	1.0855[c]	4.357	2.423	4.309	
Xe	0.087	1.125[c]	7.19	13.58	24.1	
CH_4	1.8	1.093489[b]	4.513	3.7265	6.6247	3.73
H_2	0.5	1.0912[c]	1.417	1.0607	1.8856	1.06
N_2O	0.3	1.099196[b]	5.138	5.2357	9.3076	5.23
CO	0.1	1.105329[b]	3.418	4.1873	7.4437	4.19

[a]Composition of air used as basis of Scripps O_2/N_2 scale. O_2 and CO_2 mole fractions are based on the (initial) composition of reference tank HA7017, where the O_2 abundance is based on gravimetric analysis reported in Table 9. Mole fractions for Ne,, He, and Kr from Glueckhauf (1951). The mole fractions of CH_4, H_2, N_2O, and CO are rounded estimates for typical background air. The Ar mole fraction was determined by forcing the sum to add to 10^6 using an Ar/N_2 ratio from Aoki et al (2019) of 0.0119534, which yields an N_2 mole fraction of 780840 μmol mol^{-1}. Air with the specified composition will have the same refractivity ratio as the reference for the Scripps scale, i.e. the (initial) refractivity ratio of HA7017. This is ensured by the refractivity corrections applied in the gravimetric estimation of the O_2 mole fraction of this reference (Table 8).

[b] Refractivity ratios for dry air, N_2, Ar, CO_2, CH_4, N_2O, and CO_2 are from measurements on the 61.17cm interferometer as reported in Appendix B of Keeling (1988a), where the accuracy is estimated to be 2×10^{-6} or better. The refractivity ratio for O_2 is from measurements on the 133.82 cm interferometer measured in the interferometer (see Interferometer Labbook #7, pages 70-73,76) as reported in (Keeling et al., 1998), using the same method as

(Keeling, 1988a), here expressed to one more digit. The accuracy is estimated to be ~ $\pm 4\times10^{-6}$. The O_2 measurements used Air Liquide Ultraox (>99.9999). Dry air refractivity measurements were done on tank HA7014 with 341.9 ppm CO_2 and with $\delta(O_2/N_2)$ = ~+40 per meg (relative to HA7017) in the early 1990s. These offsets from HA7017 impact refractivity ratio by less than 2×10^{-7}. Refractivity ratios reported for dry air, O_2, Ar, CO_2, CH_4, N_2O, and CO_2 are based on extrapolating a small resolved density dependence to zero density, per Keeling (1988a).

[c]Estimates except Xe from prior literature per Table tabulation in Keeling (1988b), correcting an error of 0.004 in the refractivity value for O_2. The value from Edlén (1966) has been was corrected from 15 °C to 0 °C. Xe data from Kronjäger (1936).

[d]Units: permeg/ppm for traces gases, permeg/permeg for Ar, based on $\delta(Ar/N_2)$. A positive interference factor means that an increase in the species changes the refractivity ratio in the same direction as an increase in O_2/N_2.

Table 2 provides a summary of different values of the O_2 sensitivity and CO_2 interference coefficients and reference O_2 mole fraction which have been used for data reduction in different periods. At each update, earlier data back to program inception was retrospectively reprocessed. The coefficients in current use (Aug 2017 to present) are estimates from the time of the span update in Aug 2017. These differ very slightly from the current best estimates in Table 1, reflecting earlier choices for X_{O2}, the reference Ar/N_2 ratio, and rounding errors in some of the refractivity data. The differences are very small: 0.02% in S_{O2} and 0.08% in the CO_2 interference coefficient.

Table 2. Refractivity ratio sensitivity coefficients and interference factors in different periods.

Version[a]	Reference O_2 mole fraction, X_{O2}	Sensitivity coefficient, $S_{O2}\times10^8$, ppm^{-1}	CO_2 interference, permeg/ppm
August 2017 to present	0.209436	3.3966	1.0919
April 1995 to August 2017	0.2094[b]	3.324	1.1156[c]
August 1993 to April 1995	0.2094[b]	3.324[d]	1.0104[d]
Program inception to August 1993	0.2094[b]	3.10	1.184

[a]The period reflects the time frame over which the constants were used for active data reduction. Each update entailed reworking older data, so the full time series used a uniform set of constants. Note that Aug 2017-present version differs very slightly from the best current estimates in Table 1. This reflects a decision to freeze the computer code before the final update of the best values from this report. The difference reflects a residual known uncorrected error in span of 3 parts in 10^4.

[b]Prior to Aug 2017 a value of $1/(X_{O2}(1-X_{O2}))$ = 6.04 was used in Eq. (16) defining the span sensitivity.

[c]This version of the CO_2 interference factor corrected an apparent truncation error in the refractivity ratio for CO_2, as described on page 27 of Interferometer Labbook #8, from 20 April 1995. This version of the constants was used by Blaine et al. (2005).

[d]These constants were as calculated on page 110 and 111 of Interferometer Labbook #7, from 8 August 1993. The update at that time reflected transitioning towards using a value for the refractivity ratio O_2 measured in the interferometer (see Interfermeter Labbook #7, pages 70-73,76), rather than the earlier value of Ladenburg and Wolfsohn (1932). The S_{O2} value differs very slightly from the 3.320 value subsequently presented in Keeling et al. (1998), which corrected a small error in the absolute (not relative) refractivity at 4360A of O_2 reported by Ladenburg and Wolfssohn (1932). Despite the value of 3.320 appearing in Keeling et al (1998), the value of 3.324 continued to be used for database reduction over this time frame, including by Severinghaus (1995).

Reference O_2 mole fraction

The span sensitivity per Eq. (16) in permeg/fringe depends on the absolute O_2 mole fraction of the air used as a scale reference. The Scripps O_2/N_2 scale was based at the time of program inception (circa 1990) on reporting changes relative to the air delivered from compressed air tank HA7017, which was filled in Sept. 1986 from air pumped from the Scripps pier under clean conditions. Previously, we used a rounded estimate of 0.2094 from Machta and Hughes (1970). In this revision, we use the unrounded estimate of 0.209436 from Machta and Hughes. This value differs slightly from the best estimate of 0.209448 of the O_2 mole fraction in tank HA7017 at program inception as determined from comparison with gravimetric standards (see below, Table 9). This difference has negligible influence on the O_2 sensitivity factor ($<1\times10^{-4}$). We note that the Scripps O_2 scale is not dependent on the long-term stability of the O_2 mole fraction tank HA7017, which has apparently drifted upwards due to leakage, and was never used in isolation for anchoring the scale (Keeling et al., 2007).

Uncertainty from time-invariant factors

Eq. (16) indicates that the theoretical span sensitivity includes time-invariant factors from refractivity data and the O_2 mole fraction of the air reference, X_{O2}. The combined uncertainty in these time invariant factors appears to be small. The contribution from X_{O2} must be less than 1 part in 10^4, based on the gravimetric determinations (discussed below) and noting that the factor of $(1-X_{O2})$ cancels between Eq. (16) and Eq. (3)). The most uncertain parameter is likely the absolute refractivity of O_2, which enters as a proportional factor in Eq.(3), and which has an estimated uncertainty of ~5 parts in 10^4, based on differences between measurements of Ladenburg and Wolfsohn (1932) and measurements by Stohl (1922), and Cuthbertson and Cuthbertson (1910). The error contribution from the absolute refractivity of air in Eq. (3) is ~ 2 parts 10^4 (Edlén, 1966). The error contribution from the difference in relative refractivity, $\tilde{r}_{o2} - \tilde{r}_{air}$ in Eq. (3) is estimated from observations of Keeling (1988a) to be roughly 1.5 parts in 10^4 based on combined uncertainties in $\tilde{r}_{air}$ and $\tilde{r}_{O2}$ of $\pm\ 2\times10^{-6}$ and $\pm\ 4\times10^{-6}$ respectively. Added in quadrature, these uncertainties sum to 6 parts in 10^4. The time invariant factors thus appear to contribute to less than ± 0.1% uncertainty in span.

The refractivity ratio measurements of Keeling (1988a) appear to have unprecedented accuracy, but their accuracy has not been well established by comparison to alternate measurements. For the measurement on dry air, one basis of comparison is to data from Svensson (1960), which was used to derive the formula of Edlén (1966) in the relevant

wavelength range. The Edlén (1966) formula yields a refractivity ratio from 4359.57 to 2537.27 Å that is 16×10^{-6} larger than the Keeling value in Table 1. The Keeling (1988a) measurements resolve a small pressure dependence that was previously unknown. Correcting the Keeling value to 1 atm reduces the discrepancy to 10×10^{-6}. The agreement appears to be within the uncertainties of the Svensson (1960) measurements. For O_2, the value from Keeling et al (1998) can be compared to Ladenburg and Wolfsohn (1932), whose fit (Eq. 6) yields a refractivity ratio of 1.09706 at the relevant wavelengths. Correcting for slight inaccuracy of their fit relative to their observations yields a refractivity ratio of 1.09742, which is smaller by ~500×10^{-6} than the value reported in Table 1. The agreement nevertheless appears to be satisfactory, considering that Ladenburg and Wolfsohn's method involved making independent refractivity measurements at each wavelength, with estimated errors of ~5 parts in 10^4 (see above). In any case, the comparison to Svensson (1960) appears to confirm the Keeling method to at least 10×10^{-6}. If $\tilde{r}_{air}$ and $\tilde{r}_{O2}$ in Table 1 were each inaccurate to $\pm 10\times10^{-6}$, their combined contribution to uncertainty in span would be 8 parts in 10^4.

It is worth mentioning that the refractivity and refractivity ratios for air in Table 1 are in excellent agreement with an alternate estimate, based on summing refractivity contributions from each constituent. Allowing for expected uncertainties in relative and absolute refractivities of air, O_2, Ar, and CO_2, this alternate estimate is expected to be accurate to ~ $\pm 2.6 \times 10^{-6}$ in refractivity ratio and ~ ± 3 parts in 10^4 for refractivity. In fact, the alternate estimate yields a refractivity ratio of 1.069006, (deviating by less 1×10^{-6}) and a refractivity of 2.966×10^{-4}, (deviating by less than 1 part in 10^4). Turning this around, the agreement provides a crosscheck on the uncertainty in the underlying data. For example, if all of the data were exact except the refractivity of O_2 at 4359.57 Å, which had an error of 10 parts in 10^4, the discrepancy in refractivity ratio would be 4×10^{-6} and the discrepancy in refractivity would be 6 parts in 10^4, which are significantly larger than the actual discrepancies. The agreement suggests our error estimates are conservative, as well as showing that the additive model for the refractivity of dilute mixtures (supporting Eq. (3)) is highly accurate.

Optical path difference.

Eq. (16) indicates that the theoretical span sensitivity also depends on a single time-dependent factor, the optical path difference $OPD_{samp}(\lambda_2)$, which depends on the amount of gas in the sample cell. The sample cell is operated at a stabilized pressure under constant flow, alternating between dry air samples and reference gases. The sample cell pressure is stabilized by actively controlling the pressure at a point immediately upstream of the interferometer and separated from the interferometer via a needle valve, as shown in Figure 1 of Keeling et al., (1998). The flow across this needle value produces only a small pressure drop between the control point and the sample cell. The regulation uses a sensitive differential pressure gage connected to this control point on one side and connected to sealed "reference volume", filled to

~240kPa on the other side. Flow through the sample cell is effectively determined by the pressure drop from the sample cell to the room, through the second needle valve. Sample cell pressure is measured upstream of this exhaust needle valve with a 10000 Torr MKS Baratron. This arrangement serves to simultaneously control sample cell pressure and flow, at least over short time frames. The arrangement probably partly stabilizes sample cell density in the face of laboratory temperature fluctuations, because the pressure in the reference volume will increase with lab temperature, causing a compensating increase in sample cell pressure, which will offset the density reduction caused by the temperature increase.

As described in Keeling et al. (1998), $OPD_{samp}(\lambda_2)$ is calculated on a daily basis by scaling the output voltage of the 10000 Torr MKS Baratron after subtracting the gage zero, where the gage zero is determined from the difference between the Baratron reading and wall-barometer reading of ambient lab pressure. For the zero determination, the wall barometer reading in mm Hg (torr) is corrected for temperature, using the thermometer associated with the barometer, and using the formula recommended by the manufacturer. The local gravity correction is not applied. The original Baratron was used up until 20 March 2012, when it was briefly replaced by a Paro Scientific pressure gage borrowed from Prof. Ray Weiss's lab. The Paroscientific gage was then replaced by second Baratron, which was installed on 13 April 2012 and has been used to present (July, 2019). All three of these pressure gages produce voltage output, with a nominal scaling of 1000 torr per volt.

Independent checks of the Baratron zero, determined by evacuating the cell, show that the wall-barometer method of determining the zero offset has been accurate to within ±3 Torr or better across all three gages. These zero checks were done in association with count-up calibrations (see below), but not on a daily basis. Compared to the operating pressure of 1750 torr, the zero uncertainty corresponds to span uncertainty at the ±0.2% level.

The scale factor, P_{cal}, in fringes per volt has been determined by periodically filling the sample cell very slowly from vacuum, and counting the elapsed fringes at the $\lambda_2 = 4360$Å line and simultaneously recording the Baratron output in volts. An example of such a "count-up" calibration is shown in Figure 3. Fringes have been counted using a very simple stand-alone software program for counting cycles using high and low thresholds, much like a Schmidt Trigger. Count-up runs have been done manually, usually using two people, the first person tracking the elapsed fringes on the interferometer computer screen, and the second person tracking Baratron voltages on the volt meter output display, with one person calling out "now" at the point a particular threshold was crossed, thus yielding a table of discrete (volt, fringe count) pairs that were recorded in the lab notebook. These pairs have then been fit using a linear least-squares program and the slope of the fit is taken as the P_{cal} scale factor in fringes per volt. The fits confirm that the relationship between fringe count and pressure gage voltage has remained highly linear. Except for a few obvious outlier cases, residuals to the individual linear fits in the range of typical operating sample cell pressures have been always less than ±4 fringes, corresponding to errors of less than 0.1% in $OPD_{samp}(\lambda_2)$. The short-term reproducibility in P_{cal}

determinations is also at the level of 0.05%, based on repeated count-up runs, done on the same date.

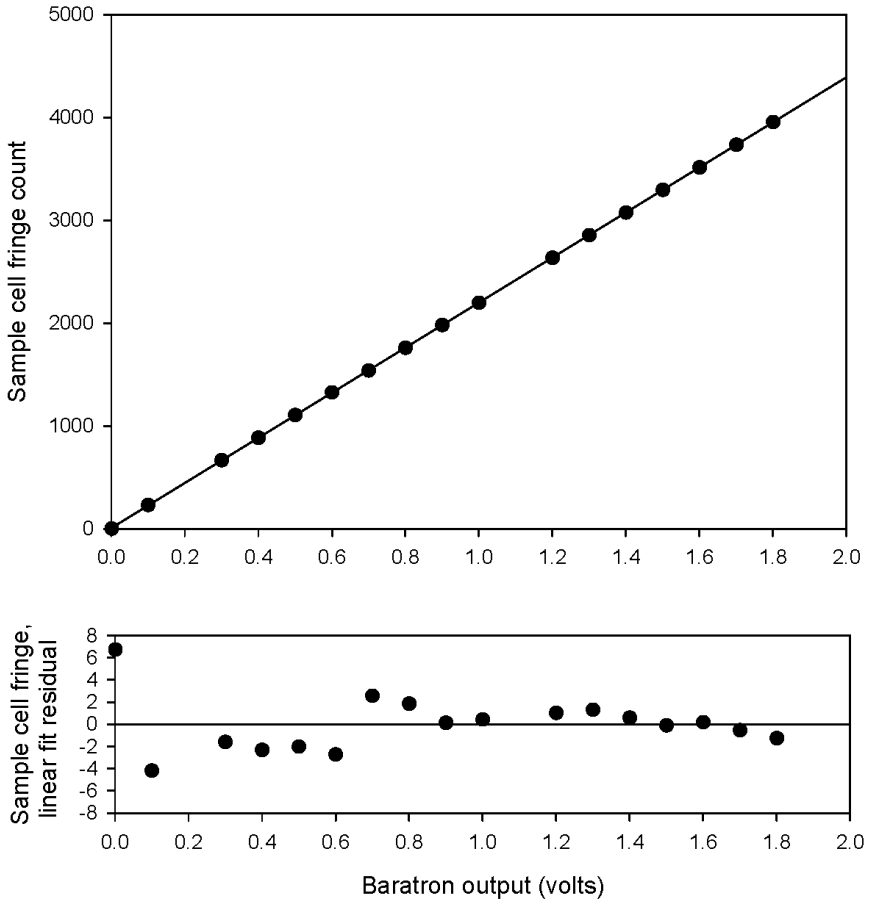

Figure 3. Example of count-up run from 22 November 1996. This run yielded a slope of 2192.9 fringes per volt. A second run on the same date yielded a slope of 2193.6 fringes per volt. The 10,000 Torr (full scale) Baratron had a nominal calibration factor of 1000 Torr per volt.

The full history of P_{cal} scale factors, one per count-up event is shown in Figure 4, which shows all results except four outlier that were easily identified by having large residuals to the fit. The highest of retained results is 2.2% higher than the lowest, with a range from 2169.7 to 2217.4 fringes per volt, and with a mean and standard deviation of 2197.7 ± 12.8.

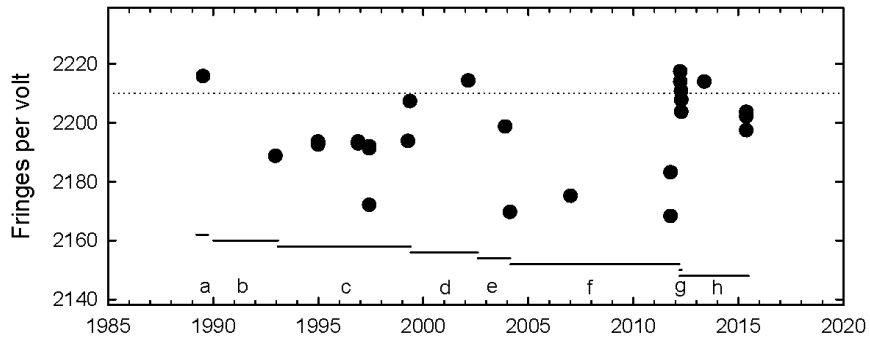

Figure 4. Measured P_{cal} scale factors, based on "count-up" runs, for determining sample cell optical path difference, $OPD_{samp}(\lambda_2)$. The dashed line shows the previously-used fixed P_{cal} value of 2210. Time periods (a-h) that punctuate possible changes in the calibration, are also shown. The y value of these periods have no significance.

The differences are much larger than the reproducibility in individual P_{cal} determinations, showing that real variations are occurring on longer time scales. Such variations might result from changes in the pressure gage performance, in lab temperature, or other factors. Periods of known notable changes that would have been expected to change these factors are documented in Table 3.

Table 3. Time periods pertinent to interferometer span calibration

Period	Start date*	End date*	Lab location	Sample cell pressure gage	Notes	$P_{cal,norm}$ scale factor, fringe/volt	Lab T offset, °C
a	1-Mar-89	1-Jan-90	Scripps, T43	MKS Baratron #1		2205.7	N/A
b	1-Jan-90	1-Jan-93	NCAR, Mesa lab	MKS Baratron #1		2202.6	0.3
c	1-Jan-93	1-May-99	Scrips Ritter Hall	MKS Baratron #1		2200.8	1.2
d	1-May-99	30-Oct-00	Ritter Hall	MKS Baratron #1	Baratron zero and span adjusted	2197.2	1.8
e	30-Oct-00	8-Feb-04	Vaughan Hall	MKS Baratron #1		2206.8	1.8
f	8-Feb-04	20-Mar-12	Vaughan Hall	MKS Baratron #1	Baratron changes behavior	2183.3	1.8
g	20-Mar-12	13-Apr-12	Vaughan Hall	Ray Weiss's Paroscientific gage		2200.2	-0.3
h	13-Apr-12	> Sept 2015	Vaughan Hall	MKS Baratron #2		2194.6	-0.3

*Dates are approximate, chosen between interferometer run dates, in order to be suitable for punctuating the database.

The practice before August, 2017 was to estimate OPD_{samp} using a fixed P_{cal} value of 2210 fringes per volt, via the following formula:

$$OPD_{samp} = 2210\ (P - P_0) \quad (17)$$

where P is the daily Baratron reading (in volts), and P_0 the observed daily zero offset. The value of 2210 fringes/volt values lies somewhat above the mean of the observed distribution in Figure 4. As a result, Eq. (17) generally causes OPD_{samp} to be overestimated and O_2/N_2 differences to be underestimated (via Eq. (14)), with a mean systematic scale error of roughly 2210/2197 = 1.0059 or 0.59%. Appendix A of Keeling et al. (1998) contains a statement implying that temperature was also used to calculate OPD_{samp}, but daily lab temperature readings were not actually incorporated. By the ideal gas law, a change of e.g. 4°C in lab temperature changes the P_{cal} scale factor by around 4/295 = 0.014 or 1.4%.

After August 2017, a different procedure for calculating $OPD_{samp}(\lambda_2)$ was incorporated that accounts more fully of changes in laboratory temperature and pressure gage characteristic. This new procedure was applied retrospectively from the program inception in 1989. This new procedure relies on lab temperature recorded routinely (e.g. for daily calibrations) from the thermometer mounted with the wall barometer. We also have available temperature readings of the main aluminum cell block of the interferometer measured using two thermocouple probes, one taped to the block near the top (TC1) and one taped near the bottom (TC2). Temperature readings from these thermocouples have been made in association with the count-up runs, but not on a daily basis. Differences between TC1 and TC2 have a mean and standard deviation of of 0.3 ± 0.6 °C.

For the new procedure, we start by defining a temperature-normalized scale factor

$$P_{cal.norm} = P_{cal}\ (\mathrm{TC2} + 273.15)/294.5 \quad (18)$$

where P_{cal} is the observed count-up slope in fringes per torr, described above, TC2 is the thermocouple reading (in °C), and 294.5K (21.4 °C) is a reference temperature based on the long-term average reading of TC2. The decision to use TC2 versus TC1 in Eq. (18) was essentially arbitrary, although TC2 showed a slightly stronger correlation with P_{cal} than TC1, as if it were a slightly more representative measure of cell temperature. The history of TC2 readings is shown in Figure 5. Eq. (18) accounts for the expected changes in P_{cal} based on the ideal gas law so that $P_{cal.norm}$ should theoretically be independent of lab temperature. Eq. (18) neglects the impact of thermal expansion of the aluminum cell block with temperature, an effect which is more than two orders of magnitude smaller, as shown by comparing the thermal expansion coefficient of aluminum (22×10^{-6} K^{-1}) with the corresponding thermal expansion coefficient for an ideal gas (1/294.5 = 0.0034 K^{-1}).

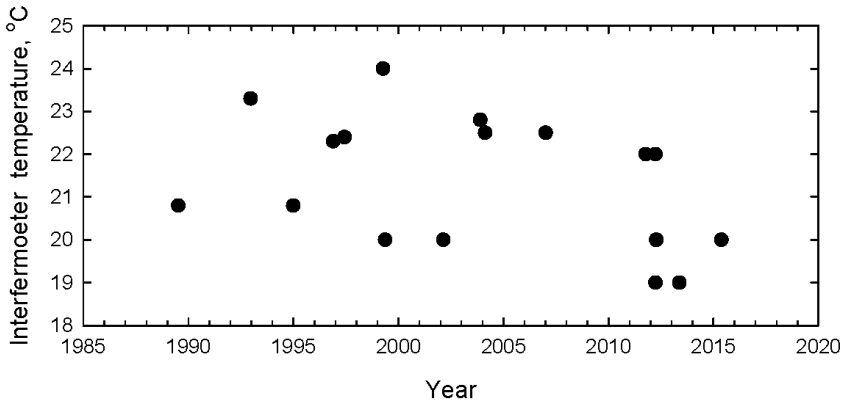

Figure 5. Interferemeter cell block temperature based on thermocouple, TC2, measured concurrently with count-up runs.

The history of $P_{cal.norm}$ scale factors from the count-up runs is shown in Figure 6. The highest of these is 1.6% higher than the lowest, with a mean and standard deviation of 2197.4 ± 8.5 fringes per volt. Compared to the results in Figure 4, the temperature normalization significantly reduced the overall variance, but did not eliminate it. Changes in pressure gage performance presumably account for some of the residual variance.

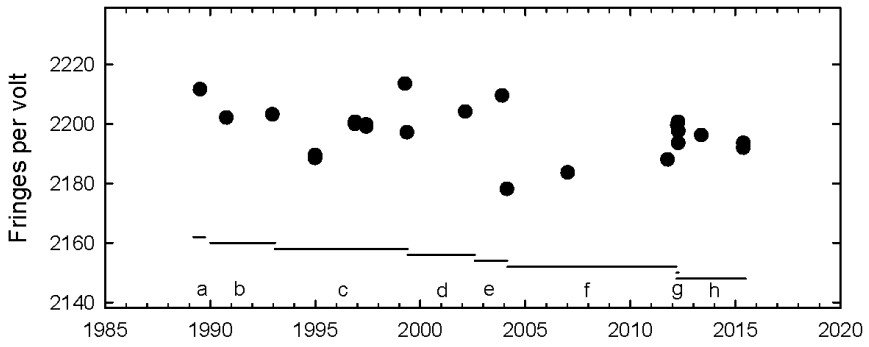

Figure 6. Same as Figure 4, except showing the temperature-normalized scale factor $P_{cal.norm}$.

Measurements of $P_{cal.norm}$ were then averaged over specific time blocks, as defined in Table 3, during which there was no indication of changes in pressure gage performance. From these results, we then compute OPD_{samp} on a daily basis using

$$OPD_{samp} = \frac{P_{cal.norm.i} \cdot (P - P_0)}{(T_{lab} + \Delta T_i + 273.15)/294.5} \tag{19}$$

where $P_{cal.norm.i}$ is the average of all the $P_{cal.norm}$ determinations made during time interval i, P and P_0 are the same as in Eq. (17), T_{lab} is the lab temperature measured daily from the temperature gage on the wall barometer, and ΔT_i is an average offset for T_{lab} and TC2 appropriate for the time interval. In applying Eq. (19), P, P_0 and T_{lab} are updated on a daily basis, while $P_{cal.norm.i}$ and ΔT_i are updated for each time interval, per Table 3. Daily values of P, P_0, and T_{lab} are shown in Figure 7.

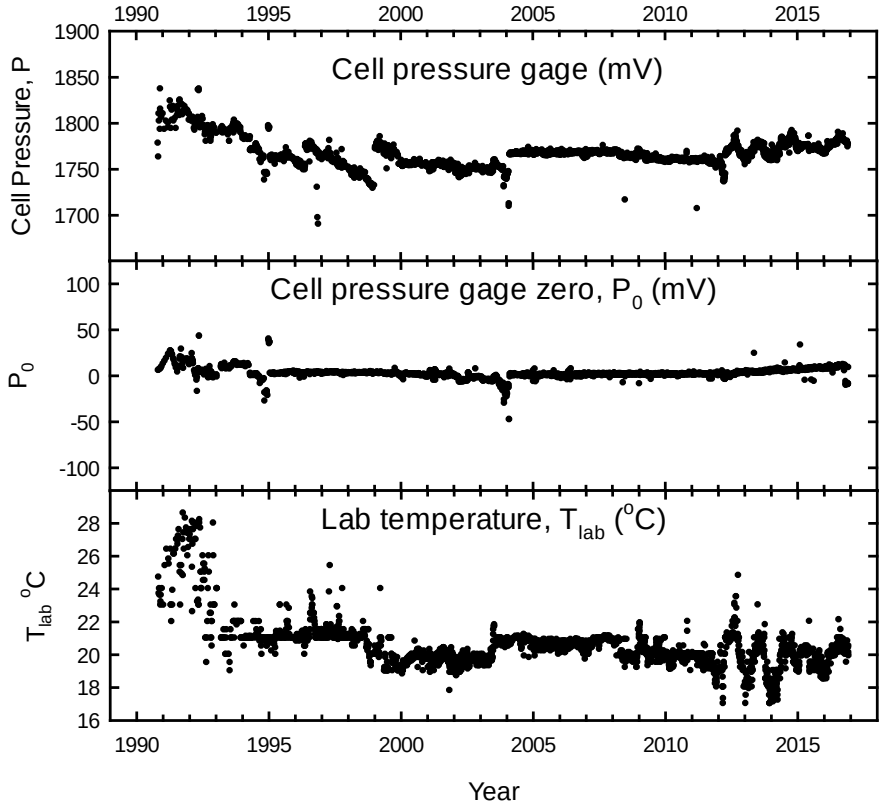

Figure 7. Daily values of P, P_0, and T_{lab}.

Eq. (19) effectively uses T_{lab} as a daily proxy for TC2, but it is clearly not a perfect proxy. Based on the available comparisons (done during count-up calibrations) the proxy appears to be valid to ±1°C. Note that the time intervals in Table 3 are punctuated both by changes in lab conditions that influenced temperatures and by changes specific to the pressure gages. The offsets between T_{lab} and TC2 were actually computed over conjoined intervals punctuated only by changes that influenced temperatures.

The accuracy of OPD_{samp}, as estimated Eq. (19), will be limited by processes contributing to scatter in Figure 6 and processes that decouple T_{lab} from the cell block temperature. From the prior analysis, the former contribution is likely around 8.5/2197 = ~ 0.4%, while the latter is around 1/294 = 0.3%. As these contributions are likely not random, we add them to estimate an overall uncertainty of around ± 0.7% in span due to inaccuracy in the OPD_{samp} determination.

This estimate may be somewhat pessimistic when averaging OPD_{samp} over longer-time scales, but larger errors seem possible on shorter periods, perhaps as large as 1%. This analysis makes it clear that uncertainty in OPD_{samp} is likely a major contributor to uncertainty in the span sensitivity.

4. Span check via O_2/CO_2 mixture addition

The span sensitivity of the interferometer was checked using a gravimetrically prepared mixture of pure O_2 and CO_2, by adding controlled amounts of this mixture into an air stream and measuring the refractivity response on the interferometer and CO_2 response on the Siemens CO_2 analyzer. The change in CO_2 is used to assess the amount of O_2 added, which allows calculating the expected change in O_2/N_2 ratio, which in turn can be compared to the actual observed change, making due allowance for the CO_2 interference on the interferometer and the non-linearity of the Siemens analyzer response. Bleed tests were carried on four dates: 2 Sept. 1994, 11 Feb. 2001, 22 July 2015, and 14 Aug. 2015, using a single gravimetric O_2;CO2 mixture prepared in 1994.

The gravimetric mixture was prepared at Jim Elkin's gravimetric lab at the NOAA Climate Monitoring and Diagnostics Lab (CMDL) on August 26, 1994 by R. Keeling (during a summer visit to NCAR) using the dual-pan Voland balance (see Gravimetric Standards lab notebook by R. Keeling). The O_2 was Alphagaz Ultra-ox with a specified purity of 99.9999%. The source of the CO_2 used was from tank #55953 from the NOAA lab with a specified purity of at least 99.99% (per Email from Elkins, 9 Nov, 2016). The isotopic composition of the CO_2 and O_2 was also not analyzed, but the effects of uncertainty in isotopic composition are small. An aluminum high-pressure cylinder was used, to which was added 161.340g of CO_2 and 442.879g of O_2, corresponding to 161.340/44.0098 = 3.666 moles of CO_2 and 442.879/31.9988 = 13.8404 moles of O_2, and O_2/CO_2 mole ratio = 3.7754. Based on the uncertainty in the individual weighings of around ±5 mg and allowing for uncertainty in the molecular weights of CO_2 and O_2 of order ±0.003% (based on typical ranges in isotopic abundance of commercial gases), the mole ratio should have a relative accuracy of around ±0.006%, i.e. better than one part in 10,000. The Siemens NDIR uses a gas-filled detector cell, and thus is selective for the dominant isotopomer $^{12}C^{16}O^{16}O$, which has a typical abundance (relative to the sum of all isotopomers) in background air ($\delta^{13}C = -7.6‰$, $\delta^{18}O = 0.26‰$ PDB-CO_2) of around 0.98410 (Keeling et al., 2016). Because the instrument is calibrated for CO_2 with background isotopic composition, a small correction is potentially required for the different isotopic composition of CO_2 in the O_2/CO_2 mixture. Commercial CO_2 is typically depleted in both ^{13}C and ^{18}O. Assuming a somewhat extreme isotopic composition of $\delta^{13}C = -50‰$, $\delta^{18}O = -20‰$ for the #55953 source tank yields a dominant isotopomer abundance of 0.98465 which compares to reference value for background air of 0.984106. In this case, the effective O_2/CO_2 mole ratio of the mixture would be smaller than 3.7754 by a factor of 0.99944. This is probably an upper bound to the correction for isotopic effects. The impact of uncertainty in isotopic composition on the interferometer span assessment is thus less than 0.1%.

The appropriate formula for computing expected changes in $\delta(O_2/N_2)$ from the addition of the O_2/CO_2 mixture is

$$\Delta\delta(O_2/N_2) = \left(\frac{\Delta X_{CO_2} \cdot R}{X_{O_2}}\right)\left(\frac{1}{1 - X_{CO2,f}(1+R)}\right) \qquad (20)$$

where ΔX_{CO2} is the change in CO_2 mole fraction on addition of the mixture, R is the O_2/CO_2 mole ratio of the mixture, X_{O2} is O_2 mole fraction of the reference for the O_2/N_2 scale (to convert ppm to per meg units), and $X_{CO2,f}$ is the CO_2 mole fraction of the air stream after the addition of the O_2/CO_2 mixture. The second factor in brackets in Eq. (20) accounts for impact of the change in total moles of air on the CO_2 mole fraction (i.e. a dilution effect). For the conditions of these experiments, this factor has a typical value of around 1.0017, i.e. it increases the predicted changes in O_2/N_2 by around 0.17%, relative to a naïve calculation which neglects the dilution effect. Eq. (20) can be shown to be equivalent to the formulation presented in Appendix 1 of Blaine (2005). For these experiments ΔX_{CO2} and $X_{CO2,}$were determined from the measured changes in CO_2 mole fraction ΔX_{CO2}.

The 1994 bleed tests are described on pages 135, 146, and 147 in the Ph.D. thesis of Jeff Severinghaus (1995). The O_2/CO_2 mixture was bled at steady flow into an air stream from a high-pressure cylinder, with the mixing done in a pressure-regulated soil chamber located upstream of the CO_2 analyzer/interferometer (Severinghaus, 1995, Figure 4.3). The tests were done with the chamber empty, so the chamber had no function other than assisting in the mixing of the gases. The setup included a changeover valve to alternately admit gas from the tank which bypassed the soil chamber into the analyzers. Differencing was done with a 10 minute changeover cycle similar to that normally used for comparing air from high pressure cylinders on the analyzers. These jogs thus resolve the offset between air delivered directly from the cylinder and (nominally) the same air with the O_2/CO_2 spike added. Jogs were performed with 5 different capillary settings, which adjusted the flow of the O_2/CO_2 spike. Jogs were also performed with the spike turned off. The original data workup (Severinghaus, 1995) neglected the possibility of a "chamber effect" or of "T" fractionation that might bias O_2/N_2 or CO_2 between the two streams in the absence of the bleed gas. The jogs with the flow turned off do allow this effect to be diagnosed, however. The workup also neglected evident drift with time in the O_2/CO_2 response in the first capillary setting and neglected the dilution factor in Eq. (20) and used an earlier version of the CO_2 interference factor. These effects have now been accounted for in the new workup presented here. The original spreadsheet documenting the workup reported in Severinghaus (1995) was recovered from Jeff Severinghaus in 2015.

The 2001 bleed tests are described in Appendix 1 of Blaine (2005), which includes tabulations of raw data (fringe differences, voltage differences) and reduced data. The flow configuration for the Blaine (2005) bleed tests was not documented but apparently involved introducing the O_2/CO_2 mixture into the air stream using a "T" located upstream of the main system changeover valve (see Keeling et al (1998), Figure 1, valve g). The bleed was evidently

turned on and off at a pace triggered manually after visual inspection that the analyzer responses had largely stabilized. The timeframe for the concentrations to stabilize after adjusting the bleed flow was considerably longer than for normal tank differencing using this changeover valve. The stabilization time appeared very similar on both the interferometer and CO_2 analyzers, as expected if caused by slow stabilization of the mixing proportions. Possibly the slow stabilization resulted from diffusive exchange in dead spaces associated with the introduction of the bleed gas. Although Blaine (2005) states that the O_2/CO_2 mixture was bled onto a stream consisting of the working tank, it is clear from inspection of the records that the tank used was the "junk" tank, i.e. the tank normally used to maintain pressure and flow during idle periods. Blaine (2005) provides an estimate of the CO_2 mole fraction of this tank of 353.48 ppm, although it is not clear if this is a preliminary (S1) or fully calibrated (S2) value (taking account of analyzer non-linearity). Working from the records of the Siemens output voltages from nearby dates, Stephen Walker recently determined the CO_2 concentration of this tank to be S2=353.53 ppm, which we use here for data reduction. In any case, the results are not highly sensitive to this small uncertainty in the CO_2 concentration of this tank.

The 2015 bleed tests on 22 July 2015, and 14 August 2015 used a dedicated "spike" system which has been used in the lab since 2007 for pure CO_2 spikes (used assess CO_2 interferences on the mass spectrometer). A drawing of the spiker configuration is shown in Figure 8.

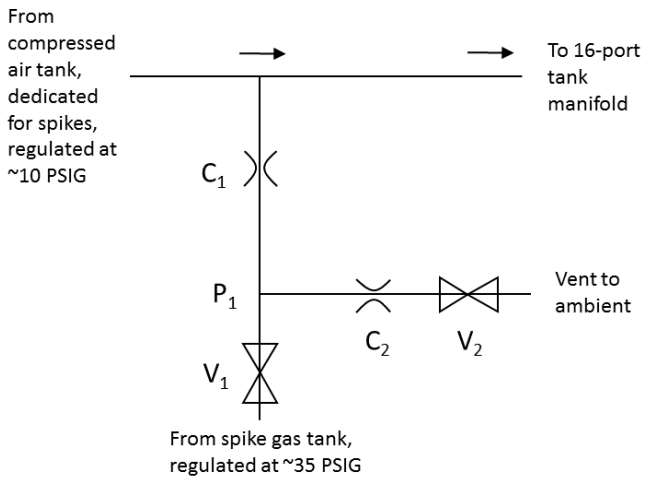

Figure 8. Flow system used to add the CO_2:O_2 mixture in 2015. C_1 and C_2 are capillaries, with C_1 being crimped for very low conductance. V_1 and V_2 are electronically activated solenoid valves. The steps in spiking are as follows: **Step 1:** V_1 and V_2 closed, 10 minutes, establishes baseline. **Step 2:** V_1 and V_2 open, 10 minutes, fast purging through V_2 establishes rapid response, P_1 rises to spike gas pressure. Step 3: V_1 closed, V_2 open, ~ 2 seconds, P1 drops to ambient, backfills with compressed air. Step 4: V_1 and V_2 closed, reestablishes baseline.

This system allows for very rapid switching on and off of the spike against a constant flow of air from a dedicated compressed air tank. Rapid switching from non-spike to spike mode

is achieved by purging the volume upstream of the capillary used to introduce the spike. Rapid switching from spike to non-spike is achieved by reversing the flow through the capillary at the switch time for a few seconds. This reverse capillary flow then drops quickly to zero, minimizing any impact of T fractionation. The spiker system is located on a dedicated line from a tank (at regulator pressure of ~10 PSIG), upstream of the main tank manifold (on position #1). Thus despite the rapid switching achieved via the capillary, a slightly longer transition time between spike and non-spike is expected compared to the normal transition time based on main system changeover valve (Keeling et al (1998), Figure 1, valve g). For this system the flow proportions are adjusted via the pressure regulator on the spike mixture. On a given date, runs were typically done with a single regulator setting.

For this report, the 1994, 2001, 2015 bleed test results were reworked, using the 1995-2015 version of sensitivity and interference coefficients from Table 2 and uniformly applying Eq. (20). The 1994 bleed tests were reworked directly from the recovered spreadsheets from Severinghaus, retaining the last 5 "jogs" for each bleed setting and also including the chamber blank jogs. This approach takes better account of the chamber blank, gives equal weight to each bleed setting, and better avoids any startup transients. The 2001 bleed tests were reworked from the tables presented in Blaine (2005), using the new estimates of the base tank using new values of the "junk" tank from Stephen Walker. Results are summarized in Table 4 and presented in Figure 1. An example of a fit to the bleed tests runs is shown in Figure 9, which can be compared to Figure 4.A1 in Severinghaus (1995).

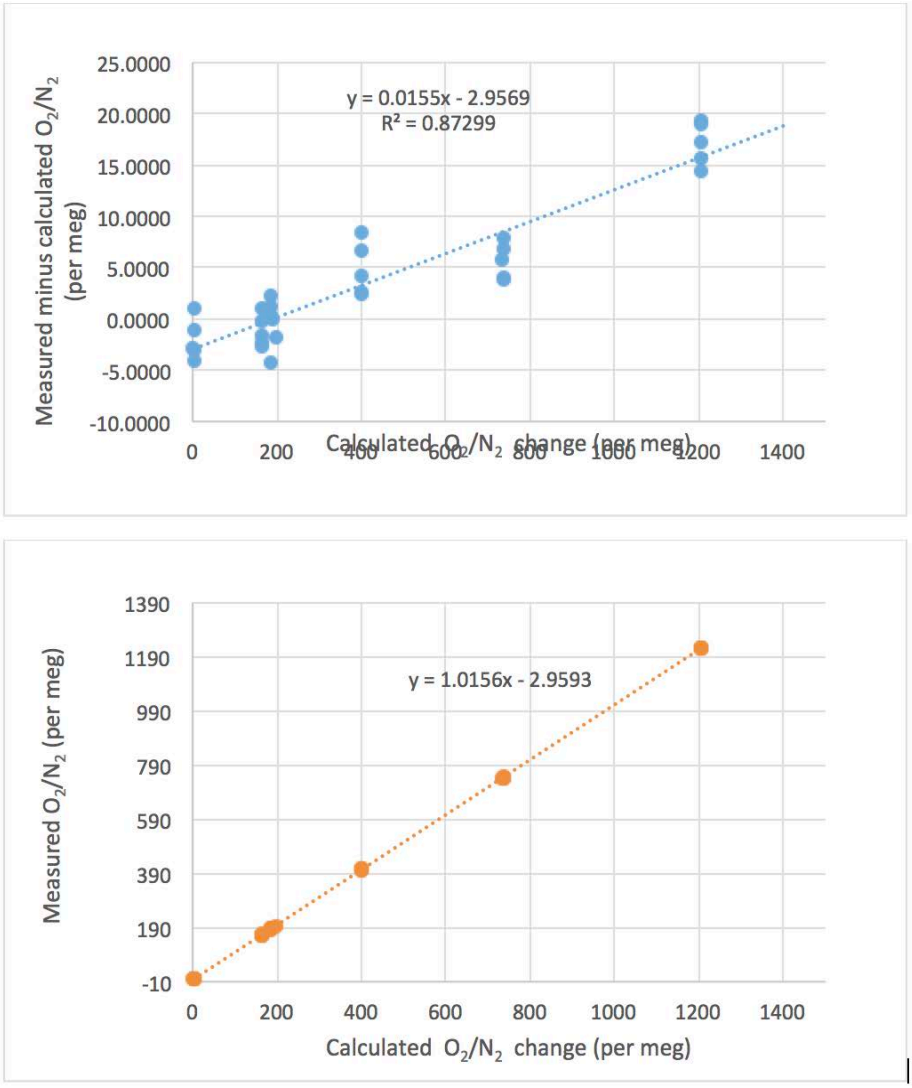

Figure 9. Measured versus calculated O_2/N_2 for the O_2/CO_2 bleed tests done by Jeff Severinghaus on 2 Aug 1994

Table 4. Span sensitivity from O_2/CO_2 additions

Date	Operator	Inferred span correction factor[1]
2 Sept 94	Jeff Severinghaus	0.9759 ± 0.0011
11 Feb 2001	Tegan Blaine	0.9807 ± 0.0054
22 July 2015	Bill Paplawsky	0.9884 ± 0.0099
14 Aug 2015	Bill Paplawsky	0.9843 ± 0.0115
9 Sept 2015	Bill Paplawsky	0.9741 ± 0.0029

[1]Correction factor computed from bleed tests of gravimetric mixture, using the "April 1995 to Aug. 2017" version of the interferometer constants from Table 2. These estimates are therefore prior to the update in the span sensitivity in Aug 2017.

5. Span check using gravimetric standards

Standards preparation

In late 1992 and early 1993, R. Keeling prepared air-like gas mixture at the standards laboratory at the NOAA-CMDL laboratory in Boulder (Novelli et al, 1991), using a dual-pan balance (Voland model HCE-10G DOW). This dual-pan balance had a capacity of 10 kg. The short-term reproduciblity for an 8 kg weight which was sequentially removed and re-weighed was approximately ±6 mg.

The standard mixtures were prepared in aluminum cylinders (Luxfur model N33) with an internal volume of 5.9 L which had been prepared by Scott Specialty Gases using their proprietary "Aculife" treatment and equipped with brass packless valves. These cylinders (with valve) have an empty weight of approximately 7.3 kg.

The weights of empty standard cylinders were compensated by placing an identical cylinder (tare cylinder) on the opposing arm of the balance. Any residual difference in weight was compensated for by adding small weights (<100g) to either pan. The tare cylinder compensates for changes in buoyancy due to changes in humidity, temperature, or barometric pressure. Weight changes caused by gas additions were determined by adding weights to the tare pan, removing weights from the sample pan, or both.

In an effort to reduce random errors, sample cylinders were weighed eight to ten times at each stage in the filling sequence. Each weighing was preceded and followed by a weighing of a third nominally-identical “carrier” cylinder such that the weight of the sample cylinder was essentially determined relative to the carrier cylinder. Each weighing consisted of hanging and arresting the arm of the balance 6 to 10 times, and averaging the readings from all but the first two or three hangings.

The procedure for preparing standards involved the following steps: (1) evacuating the cylinder to 5 μHg and taring the cylinder on the Voland balance, (2) filling the cylinder with a mixture of CO_2 in Ar and measuring the weight gain on the Voland balance, (3) adding pure O_2 to the cylinder and measuring the weight gain, (4) adding pure N_2 and measuring the weight gain, and (5) horizontally rolling the cylinder on a tumbler to achieve mixing. The mixture of Ar in CO_2 was prepared using an analogous procedure. In order to control the amount of each gas added, the cylinders were placed on a platform balance (Sauter model E1210) with a resolution of 1 g. The gas was transferred to the tanks through a short 1/16" diameter line which was oriented horizontally so as to minimize vertical forces caused by changes in the pressure in the line during filling. The transfer line was thoroughly purged with the relevant gas prior to transfer.

Six such standard mixtures were prepared. In computing the absolute composition of the mixtures, corrections were applied for the effects of impurities in the source gases, and for

changes in tank buoyancy due to expansion, as described below. The calculations of the abundances of gases in the mixtures are summarized in Table 5.

Table 5. Summary of calculations of gravimetric standards[a]

Cylinder ID#		34289	002430	37020	37041	37027	37022
CYL	Initial cylinder weight (tared)	3.658	-34.656	-23.9115	-19.534	-21.282	-11.218
PAR1	Initial weight plus Ar, CO2 mixture (first weighing)	16.853	-22.598	-12.134	-7.9	-9.932	0.056
PAR2	Initial weight plus Ar, CO2 mixture (second weighing)[b]	16.826					
PO2	Initial weight plus Ar, CO2, O2 mixture	246.597	185.614	187.436	194.196	184.8315	198.711
PN2	Initial weight plus Ar, CO2, O2 and N2 mixture	994.962	865.986	836.75	855.94	820.216	846.864
N2 source cylinder ID#		300T-0832	6613	6613	38722	38722	38722
fAr	Ar fraction (by mass) of Ar-CO2 mixture	0.959816	0.959816	0.959816	0.959816	0.959816	0.959816
fCO2	CO2 fraction (by mass) of Ar,CO2 mixture	0.040184	0.040184	0.040184	0.040184	0.040184	0.040184
MWN2	Molecular mass of N_2	28.013238	28.013451	28.013451	28.013451	28.013451	28.013451
MWO2	Molecular mass of O_2	31.998822	31.998822	31.998822	31.998822	31.998822	31.998822
MWAR	Molecular mass of Ar	39.948	39.948	39.948	39.948	39.948	39.948
MWCO2	Molecular mass of CO_2	44.0095	44.0095	44.0095	44.0095	44.0095	44.0095
BUOY	Buoyancy correction (has units of g/mole)	0.000578	0.000578	0.000578	0.000578	0.000578	0.000578
IMO2	O_2 impurity of N_2	0.00000568	0.00000023	0.00000023	0.0000004	0.0000004	0.0000004
IMAR	Ar impurity of N_2	0.00005849	0.00007963	0.00007963	0.00007978	0.00007978	0.00007978
N2Frac	Nitrogen fraction of N2 gas	0.9999358	0.99992014	0.99992014	0.99991982	0.99991982	0.99991982
MWN2eff	Average molecular mass of N2 plus its impurities	28.0139587	28.01440226	28.01440226	28.01440473	28.01440473	28.01440473
MOLN2EFF	Total moles of N2 plus its impurities	26.71456	24.28701	23.17834	23.62205	22.68110	23.13690
MOLN2	Total moles of N_2	26.71284	24.28507	23.17649	23.62016	22.67928	23.13504
MOLO2	Total moles of O_2	7.18089	6.50699	6.23691	6.31586	6.08670	6.20832
MOLAR	Total moles of Ar	0.31860	0.29165	0.28482	0.28141	0.27452	0.27273
MOLCO2	Total moles of CO_2	0.01205	0.01101	0.01075	0.01062	0.01036	0.01029
TOTALMOL	Total number of moles	34.22438	31.09472	29.70898	30.22805	29.05087	29.62638

[a]Weights in grams, impurities in mole fraction.

[b]For tank 34289, several months elapsed between the CO_2/Ar fill and the subsequent fillings. The 1st weighing was used to establish the weight gain associated with the CO_2/Ar fill, the 2nd weighing to establish the weight gain associated with the O_2 fill. Cylinder weights in grams.

Source gas impurities and isotopic composition

The source gases are detailed in Table 6. The O_2 and Ar source gases were obtained from the vendor at very high purity, for O_2 > 99.9999%. Three different source cylinders of N_2 were used, of variable purity. Samples from all three N_2 tanks were decanted into evacuated 30 SCF cylinders and stored at Scripps for follow-on analysis. These three N_2 tanks plus the original O_2 and Ar source gases were still being stored at Scripps as of 2018.

Table 6. Gravimetric source gas characteristics

Tank ID	Species	Vendor	Vender specifications	Further analysis	Molecular Mass[5]
548348Y	O_2	Air Liquide	Ultraox (>99.9999%)	$\delta^{18}O$ = 3.25‰[7]	31.998822
IA-018171[1]	Ar	Scott Specialty Gases	Ultra High Purity (> 99.999%)		39.948
55953[2]	CO_2	Airco/BOC	High purity (>99.99%)		44.0095
300T-0832[3]	N_2	US Welding	Unknown	$\delta^{15}N = -2.02$‰[4] O_2 = 5.68 ppm[6] Ar = 58.49 ppm[6]	28.013238
006613[3]	N_2	Scott	"Prepurified N_2", O_2 < 5 ppm, H_2O < 4 ppm	$\delta^{15}N = -0.159$‰[4] O_2 = 0.23 ppm[6] Ar = 79.63 ppm[6]	28.013451
38772[3]	N_2	Scott	"Prepurified N_2", O_2 < 5 ppm, H_2O < 4 ppm	$\delta^{15}N = -0.203$‰[4] O_2 = 0.40 ppm[6] Ar = 79.78 ppm[6]	28.013451

[1]Although the purchase records of this tank could not be located, the tank still existed at Scripps as of Nov. 2016 and was clearly marked as Scott Specialty Gases UHP Ar. More recent literature from Scott Specialty Gases list the purity of UHP as 99.999%. Both Jim Elkins and R. Keeling remember acquiring this tank back in ~1992 specifically for the gravimetric work. R. Keeling remembers that the grade was essentially the highest purity that was readily obtainable commercially at the time, e.g. 99.999% or better.

[2]Page 144 of the gravimetric notebook lists this tank as 55935, but follow-up Emails with Jim Elkins and Brad Hall of NOAA GMD in Nov. 2016 confirmed that the tank, which still existed at NOAA in Nov. 2016, actually was number 55953. The last two digits were evidently transposed in the notebook. These Emails confirmed that the tank purity was at least HP (high purity > 99.99%) but possibly was UHP (>99.999%).

[3]On page 133 of the gravimetric notebook it is clarified that, on 23 Jan 1993, a fraction of the content of these tanks was "decanted" into evacuated smaller 30 SCF cylinders for archiving material, allowing the original tanks to be returned to the vendor while preserving sample for follow-on analysis. Content of tank 300T-0832 was decanted into tank FF7909. Content of tank 006613 was decanted into tank FF3884. Content of tank 38772 was decanted into tank FF3672.

[4]Measured in the laboratory of Jeff Severinghaus by Ross Beaudette and communicated by Email to R. Keeling on 25 Jan 2017. The isotopic standard for the reported $\delta^{18}O$ and $\delta^{15}N$ values are O_2 and N_2 in background air. For N_2, the measurements were done on 30 SCF archival tanks, see footnote 3.

[5]For O_2 and N_2, molecular mass is calculated from measured isotopic abundances $\delta^{18}O$ and $\delta^{15}N$ (see previous column) following calculations in Tohjima et al. (2005), assuming $\delta^{17}O = 0.5\times\delta^{18}O$, where $\delta^{18}O$ and $\delta^{17}O$ are relative to background air. The calculation relates the O_2 isotopic composition of background air to VSMOW following Tohjima et al. (2005). The calculation uses constants in de Laeter et al. (2003), which provides a convenient summary of the isotopic abundances of isotopic reference materials (air for N_2, VSMOW for O_2) and isotopic atomic masses, as used by Tohjima et al (2005). For Ar and CO_2, the molecular mass assumes normal isotopic abundance, following Table 4 of de Laeter et al (2003).

[6]Measured from smaller 30 SCF cylinders (see Footnote 3) in the Chemical Sciences Division of the National Institute for Standards and Technology in Gaithersburg, MD in 2018 by Kimberly Harris.

[7]Measured in the laboratory of Jeff Severinghaus by Ross Beaudette and communicated by Email to R. Keeling on 25 Jan 2017. Measurements were done on 30 SCF archival tanks, see footnote 3. Isotopic reference for these measurements was background air.

The isotopic composition of the N_2 derived from the three smaller N_2 tanks and isotopic composition of the O_2 from the original O_2 source tank was measured by Ross Beaudette in Prof. Jeff Severinghaus's lab at Scripps Institution of Oceanography in late 2016 and early 2017 on a Thermo-Fischer mass spectrometer. These analyses reported isotopic differences (δ values) using natural background air as the isotopic reference. The results of these isotopic measurements and the calculation of molecular masses is detailed in Table 6.

Buoyancy correction

The buoyancy correction was assessed on a similar model N33 tank by filling this tank with compressed air, immersing the tank in (degassed) water in a sealed basin with a graduated tube at the top, and then venting the tank through a separate non-wetted air line. As the pressure dropped, the change in volume of the cylinder was determined by recording the change in water level on the graduated tube. The volume versus pressure relationship was highly linear. These results yielded a linear expansion coefficient of 95 cm^3 per 1000 PSIG valid over the range from 0 to 2000 PSIG. This translates into a correction to the apparent weight of approximately 5.8×10^{-4} g per mole of gas based on a typical air density of 0.00096 g cm^{-3} for Boulder. In fact, the buoyancy correction is virtually negligible and amounts to only 4×10^{-7} in the O_2 mole fraction. The buoyancy correction is small because it causes nearly proportional changes in the apparent weights of O_2 and N_2, owing to the similarity in their molecular masses.

Surface adsorption correction

The effects of surface adsorption on the O_2/N_2 ratio of air in the tank was assessed by evacuating a standard cylinder, transferring air into it from a particular source tank, and then comparing the concentration in the standard tank against the source tank using procedures described in section IV above. Unfortunately, these tests yielded ambiguous results. In two such experiments, the O_2/N_2 ratio in the standard cylinders were lower by 37 per meg and 28 per meg, respectively, and in two additional experiments the O_2/N_2 ratio in the standard cylinder were higher by 15 to 20 per meg. This variability was possibly caused by fractionation occurring during the transfer processes. Simple tests using the high pressure "T" (described in Keeling et al., 1995) showed that such fractionation does indeed occur. A reasonable estimate is that the surface effect is 0±20 per meg, where the uncertainty reflects the inability to reliably transfer air from one tank to another without fractionation.

Refractivity corrections for gravimetric cylinders

In order to compare the gravimetric-based O_2 mole fractions with the O_2/N_2 determinations on the interferometer, it is necessary to apply corrections for differences in inert gas and trace gas composition between the mixtures and realistic air. In the approach taken here, each gravimetric mixture was conceptually paired with a hypothetical normalized air mixture, with the same O_2 mole fraction, but containing trace gases and an Ar/N_2 ratio corresponding to "normal" air. The difference between the refractivity ratio of each gravimetric mixture and its corresponding normalized mixture is then applied as a correction to the measurements on the interferometer. After applying this correction, the gravimetric mixtures can then be treated as if they were comprised of natural air with an altered O_2 mole fraction. Measurement of these tanks on the Scripps O_2 scale, which uses real air as a reference, can thus be used to determine the absolute O_2 mole fraction of Scripps scale reference as well as providing an independent check on span sensitivity. (Note that this approach cannot rely on Eq. (3) to calculate interferences, because Eq. (3) assumes fixed relative abundances rather than fixed O_2 mole fraction upon addition or removal of other gases).

The difference in the refractivity ratio between each gravimetric mixture and its corresponding normalized mixture was computed using the additive model for mixtures (see Eqs. (5) and (7) in Keeling ((1988b)), using refractivity data in Table 1. The normalized mixture is assumed to be comprised of N_2, O_2, Ar, CO_2, Ne, He, Kr, Xe, CH_4, H_2, N_2O, and CO with abundances as per Table 7. The CO_2 mole fraction in Table 7 is from tank HA7017, the original reference for the Scripps scale. The normalized Ar/N_2 ratio is from Aoki et al (2019). The ratios of other noble gases to N_2 are from Glueckauf (1951). The mixture defined by Table 7 has one remaining degree of freedom, corresponding to the unspecified O_2 mole fraction. This O_2 mole fraction is assigned from the corresponding gravimetric mixture.

Table 7. Refractivity and abundance data used for correcting gravimetric standards to "normalized mixture".

Relative molar abundances in normalized mixture	
Ar/N2 ratio	0.0119534
CO2 mole fraction	0.00036329
Ne/N2 ratio	0.00002328
He/N2 ratio	0.00000671
Kr/N2 ratio	0.00000146
Xe/N_2 ratio	0.000000111
CH4 mole fraction	0.0000018
H2 mole fraction	0.0000005
N2O mole fraction	0.0000003
CO mole fraction	0.0000001

Calculations summarizing these refractivity ratio corrections are presented in Table 8, with the resulting correction expressed in per meg units. For all six gravimetric mixtures, the corrections are quite similar, falling within the range of +36 to +48 per meg.

Table 8. Inert and trace gas corrections for gravimetric cylinders

Cylinder number		34289	002430	37020	37041	37027	37022
XN2	N2 mole fraction of gravimetric mixture	0.78052088	0.78100303	0.78011740	0.78139861	0.78067498	0.78089328
XO2	O2 mole fraction of gravimetric mixture	0.20981798	0.20926344	0.20993351	0.20894025	0.20951879	0.20955374
XAR	AR mole fraction of gravimetric mixture	0.00930911	0.00937945	0.00958712	0.00930971	0.00944949	0.00920551
XCO2	CO2 mole fraction of gravimetric mixture	0.00035204	0.00035408	0.00036197	0.00035142	0.00035674	0.00034747
N436STD	Refractivity of standard mixture at 436 nm	0.0002965528	0.0002965668	0.0002965465	0.0002965763	0.0002965592	0.0002965609
N254STD	Refractivity of standard mixture at 254 nm	0.0003170202	0.0003170296	0.0003170147	0.0003170365	0.0003170240	0.0003170263
RSTD	Refractivity ratio of standard mixture	1.069017938	1.068999104	1.069021903	1.068988114	1.06900779	1.069008936
N436NOR	Refractivity of normalized mixture at 436 nm	0.0002965489	0.0002965637	0.0002965458	0.0002965724	0.0002965569	0.0002965560
N254NOR	Refractivity of normalized mixture at 254 nm	0.0003170162	0.0003170264	0.0003170141	0.0003170324	0.0003170217	0.0003170211
RNOR	Refractivity ratio of normalized mixture	1.069018195	1.068999355	1.069022121	1.068988376	1.069008030	1.069009218
RNOR-RSTD	Refractivity ratio difference	2.570E-07	2.509E-07	2.180E-07	2.615E-07	2.400E-07	2.820E-07
COR	Correction in per meg[a]	45.7	44.6	38.7	46.5	42.7	50.1

[a]Computed from the refractivity ratio difference using Eq. (14) with $S_{O2} = 3.397\times10^{-8}$ (Table 2) and $X_{O2} = 0.209448$ (Table 1).

The contribution from different constituents are as follows: The CO_2 contribution to the correction varies between +3 and +37 per meg, depending on the tank. The correction for offsets in Ar/N_2 between the gravimetric tanks and the normalized mixture varies from -8 to + 15 per meg. The combined correction for Ne, He, and Kr is essentially constant at -1.7 per meg, and combined contribution from the trace gases CH_4, H_2, N_2O, and CO is effectively constant at +20 per meg.

To apply these corrections to the interferometric determinations on the gravimetric cylinders, it is first necessary to "undo" the normal CO_2 interference correction, because the CO_2 correction would otherwise be applied twice. In the normalized-mixture calculations, the O_2 mole fraction is held constant while CH_4, H_2, N_2O, and CO are set to their normalized mole fractions. The mole fractions of N_2 Ar, Ne, He, Kr, and Xe in the normalized mixture are then determined algebraically by two constraints: (1) the ratios to N_2 are given as in Table 7, (2) the mole fractions of all species sum to unity.

Analysis of gravimetric standards on interferometer

The six gravimetric tanks were analyzed on the interferometer system in 1992, 1993, 2012, and 2015, as summarized in Table 9. The interferometer measurements were worked up using the current (Aug 2017-present) version of the sensitivity coefficients (Table 2) and the optical path difference (OPD).

Table 9. Interferometric runs, final (S2) values for CO_2 and O_2/N_2.[a]

Interferometer runs

Tank ID number	O_2 mole percent	Analysis, Nov 1992 - Jan 1993[b]			Analysis, 21 Dec 1993			Analysis, 18 Sep 2012			Analysis, 10 Mar 2015		
		CO_2 ppm	O_2/N_2 permeg	O_2/N_2 norm[c]	CO_2 ppm	O_2/N_2 permeg	O_2/N_2 norm[c]	CO_2 ppm	O_2/N_2 permeg	O_2/N_2 norm[c]	CO_2 ppm	O_2/N_2 permeg	O_2/N_2 norm[c]
34289	20.9818	350.54	2216.3	2245.9	350.45	2200.4	2229.9	350.49	2230.4	2259.9	350.44	2220.5	2249.9
2430	20.9263	352.86	-1099.3	-1068.2	352.79	-1129.9	-1098.9	352.86	-1122.8	-1091.8	352.80	-1114.4	-1083.3
37020	20.9934	360.94	2848.5	2882.3	360.91	2872.7	2906.9	360.97	2904.3	2938.5	360.92	2896.8	2931.0
37041	20.8940	350.29	-3080.0	-3049.9	350.17	-3109.5	-3079.6	350.27	-3108.5	-3078.5	350.14	-3093.5	-3063.6
37027	20.9519	355.52	345.1	377.1	355.47	339.3	371.3	355.55	363.9	396.1	355.50	359.8	391.8
37022	20.9554	346.12	636.7	665.8	346.08	641.2	670.3	346.17	655.2	684.3	346.08	660.1	689.1

Linear fit results

Slope (per meg^{-1})[d]	1.671E-07 ± 1.3E-09	1.659E-07 ± 1.1E-09	1.650E-07 ± 1.0E-09	1.657E-07 ± 1.1E-09
Intercept[d]	0.209447 ± 0.000002	0.209449 ± 0.000002	0.209446 ± 0.000002	0.209446 ± 0.000002
Span sensitivity correction factor[e]	1.0093 ± 0.0082	1.0018 ± 0.0070	0.9964 ± 0.0061	1.0006 ± 0.0068

[a]Results for O_2/N_2 in per meg are based on data reduction algorithms in use after the span sensitivity update described in this report. Based on "results.tanks.csv" from the 2019-08-01 archive.

[b]Between Nov. 30 1992 and Jan 16, 1993 all six tanks were run at least once, but not on the same dates. For tanks 34289, 2430, and 37020, which were run twice in this interval, the result shown is the average of the two runs.

[c]Normalized O_2/N_2 value, calculated by undoing the CO_2 interference and applying the correction (COR) from Table 8: O_2/N_2 norm = O_2/N_2 +1.0919·(CO_2 – 362.29) + COR

[d]Linear least-squares fit ($y = mx + b$) between O_2 mole fraction (y) and O_2/N_2 corr (x), with slope m and intercept b. Errors are based on residuals to fit.

[e]Ratio of fitted slope (m) to the expected theoretical slope m', where $m' = X_{O2} \cdot (1 - X_{O2}) \times 10^{-6} = 1.6558 \times 10^{-7}$, based on $X_{O2} = 0.209448$ via Eq. (5).

The $\delta(O_2/N_2)$ values, derived by working up these runs as if they were normal air samples, were then adjusted with the corrections described in the previous section. The O_2 mole fractions in these tanks, based on their gravimetric preparation, were then fit against the corrected $\delta(O_2/N_2)$ values to yield a slope and intercept. The slope is directly related to the span sensitivity, while the intercept is related to the absolute O_2 mole fraction corresponding to the zero value of the Scripps O_2 scale. The uncertainties in slope and intercept are derived from the

parameters of the least-square fit. The residuals are strongly correlated for all analyses dates because they are partly related to random errors in the gravimetric data which are fixed for each tank. The fitted slopes tend to confirm the revised span sensitivity to within ±1%. Averaging the runs in 1992 and 1993 (when the gravimetric tanks were relatively new) yields a mean correction factor of 1.0055 ± 0.008, where the uncertainty is assumed to be same as for an individual run. Here a factor greater than unity implies that reported difference of 100 per meg corresponds to an actual difference that is greater than 100 per meg. The intercept yields an O_2 mole fraction corresponding to the zero of the Scripps O_2 scale of 0.209448. The composition of the normalized mixture consistent with this O_2 mole fraction is given in Table 1. This mixture has an O_2/N_2 ratio of 0.268238 mol mol^{-1}.

Perceptive readers may note that the reference O_2 mole fraction X_{O2} = 0.209448 which resulted from these calculations was also used as an input via the span sensitivity from Eq. (16). This apparent circularity is not significant, however, because the intercepts calculated in Table 9 are not sensitive to the value adopted for the span sensitivity, and because the span sensitivity correction factors (Table 9) are not sensitive to small changes in the reference X_{O2} value.

Precision of gravimetric standards

Based on the precision of an individual weighing, and the number of repetitive weighings done for each sample, we expected that the weighings should establish O_2 content of each standard to a precision of approximately ±0.000004 in the O_2 mole fraction. Uncertainty of order ± 0.000001 to ± 0.000002 is expected from the interferometric analyses. The residuals from the fits in Table 9 imply a precision of about ±0.000006%, which is in reasonable agreement with the expected overall precision.

6. Scale contraction from incomplete sample/reference replacement

The analysis of tanks against each other on the interferometer is based on 10 minute differencing. Although the sweep-out transients associated with the differencing are largely masked out by the data reduction algorithms, it is inevitable that tank differences will be slightly underestimated due to residual “tailing”, leading to slight scale contraction.

One constraint on this scale contraction effect is provided via comparison between the theoretical span sensitivity and the O_2:CO_2 and gravimetric crosschecks in Figure 1. For both crosschecks, the “known” change in O_2/N_2 corresponds to the change in source gas composition upstream of the interferometer and is therefore independent of the dynamics of gas replacement in the interferometer. The relatively good agreement between these crosschecks and the theoretical relation (after updating parameters as in Section 3) suggest that any scale contraction due to residual tailing must be less than 1%.

Scale contraction for tank comparisons

To provide further insight into tailing effects, we bin-averaged a large number (557) of working tank versus “oxspan” tank jogs to yield a very finely resolved sweep-out curve at the

30-second resolution of the interferometer raw data stream. (The "oxspan" is a tank introduced during daily calibrations with very negative $\delta(O_2/N_2)$ relative to concurrent background air, mainly used as a cross check on the Isoprime analyzer). Figure 10 shows such data for both the interferometer and the Siemens CO_2 analyzer, located upstream of the interferometer. These curves are scaled to yield exactly 1.0 for the highest bin-averaged point and 0.0 for the lowest bin-averaged point. Data points that are within the time masks over which data is averaged in our normal data reduction algorithms to compute the jog differences are shown with larger black symbols.

To quantify these bin-averaged results, we fit a line to the retained (large black) points but also masking out small interferometer spikes that are evident at t=600 and t=1200 seconds (see next paragraph). For the Siemens analyzer the change over this averaging window, based on this line, is about 0.1% of the full transition. For the interferometer, the change is roughly 0.3% of the full transition. These results suggest that scale contraction effects are likely much smaller than 1%. But a limitation of this analysis is that it doesn't address further tailing that might have occurred if the jog had extended longer than 10 minutes.

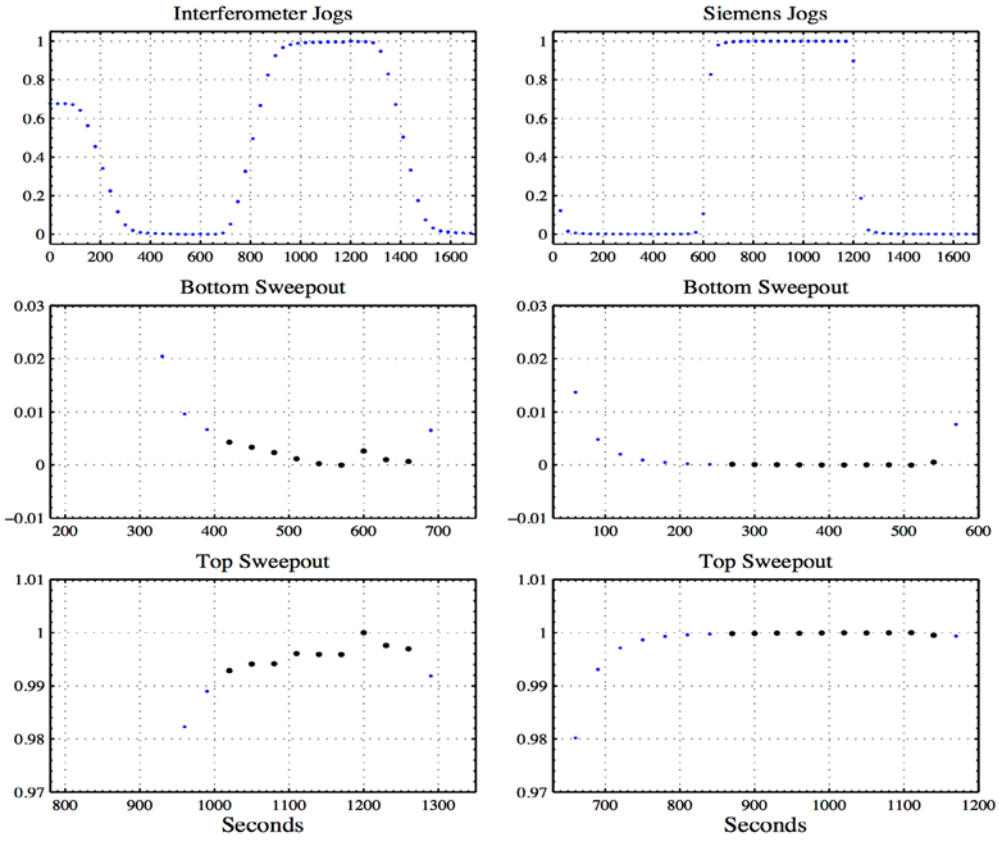

Figure 10 Top panels show bin-averaged sweepout curves normalized to give 1.0 and 0.0 for the maximum and minimum points. The bottom panels show zoomed visualizations of downward and upward transitions. The points retained for calculating jog difference as black circles. Points that are masked out are shown as smaller blue circles. Left panels show jogs for the interferometric O_2 analyzer and right panels show transitions for the Siemens CO_2 analyzer.

The spikes noted in the previous paragraph occur exactly the point in time when the main changeover valve is switched, but are not masked out in data reduction because the masks take account of the several-minute delay for arrival of new gas in the interferometer after the switch. The spikes might be due to tiny pressure changes that propagate quickly through the full system (faster than the gas itself) or might be due to an electrical effect which is picked up in the fringe signals. As can be seen in Figure 10, these spikes shift the high and low jogs in the same direction, so must cancel in the difference. These spikes, which are very small in any case, therefore cannot impact scale contraction. The spikes do interfere slightly with the diagnosis of the tailing effect, which is why we weed them out here.

To address tailing beyond the 10-minute point, we carried out runs (in Aug. 2015) using a pair of tanks that were quite far apart in O_2/N_2 (working tank vs. oxspan) but for these runs, we used a switching interval of 20 minutes, instead of the normal 10 minute interval. The tank difference was first calculated using the normal mask after each valve switch, mimicking the normal sweep-out and ignoring the second half of the run. These same jogs were then also analyzed using only data from the second half of the 20-minute segment, effectively delaying the mask by 10 minutes and thereby adding 10 minutes to the time allowed for gas replacement. The runs were carried out for a total of 3 jogs. For these, the ratio of the 10 minute to 20 minute jog differences on the interferometer were 0.9946, 1.0025, and 0.9866, suggesting a mean scale contraction of 0.5% and a standard error of ±0.5%. These differences account for incomplete sweep-out on both the positive and negative transitions, so correspond to the correction factor needed for actual tank differences. Under the assumption that using the second 20-minute cadence achieves 100% replacement, these ratios can be used as estimates of the scale contraction using our normal 10-minute switching. In other words, it appears that differences in O_2/N_2 in tanks measured on the interferometer may be underestimated by ~0.5 ± 0.5% due to scale contraction effects. This is consistent with the O_2:CO_2 and gravimetric crosschecks which suggest that any scale contraction effect is smaller than 1%, and it consistent with the small amount of drift seen within the masking intervals.

In summary, we believe that scale contraction on the interferometer due to “tailing” on tank comparisons is at the level of 1% or smaller. This conclusion is supported by four independent measures: (1) O_2:CO_2 cross checks, (2) gravimetric cross checks, (3) sweep-out shape, (4) comparison of longer and shorter switching transitions. Our best estimate of the effect is ~0.5 ± 0.5%, i.e. actual reported differences in O_2/N_2 may be too small by 0.5% ± 0.5%. At present, we do not correct for this small effect. If necessary, the effect could be better quantified by carrying out a larger number of comparisons with shorter and longer switching transitions.

Scale contraction for flask analyses

The above tests address the impacts of sweep-out effects for tank comparisons, but don’t address additional sweep-out corrections associated with analyzing flasks, which are subject to a different kind of tailing effect. As described in Keeling et al (1998), the flasks for O_2/N_2 analysis have two stopcocks. During analysis, the working tank is introduced into the inlet stopcock

while a mixture of working tank and flask air then exits via the outlet. The mixture is initially nearly pure flask air, but an increasing proportion of working tank air is present in the outflow over time. The data-reduction method requires interpreting this sweep-out curve to recover the signal that would have been obtained if 100% flask air were obtained at the flask outlet.

Prior to Feb. 2001, the flasks peaks were hand-ruled on the chart, and the flask sweep-out correction involved multiplying these hand-ruled peaks by a scale factor that was "calibrated" based on running "known" flasks which had been purged (on the analysis rack) from a tank well characterized in O_2/N_2 and CO_2.

This hand scaling method was replaced with a curve fitting method implemented from flasks analyzed from Feb. 2001, onwards (see Section 7). This fitting method uses fixed sweep-out templates, determined by bin-averaging many sweep-out curves for flasks. This template, which is assumed to be identical for flasks mounted in the three rack positions, is fit to the actual flask sweep-out data and used to determine the "peak" point on the sweep-out curve, conceptually similar to the hand method done by prior to Feb 2001. The shape of the sweep-out template is adjusted to vary with flask pressure because bin averages of flasks at different pressures showed slight changes in shape. The difference between flasks and working tanks is then scaled up by a factor of 1.14 to correct for partial working tank break-through. This value of 1.14 is supported by an updated sweep-out calibration method, implemented in Nov. 2002. The updated method involves using two working tanks, used alternately on consecutive dates. One of these working tanks is prepared to be slightly high in O_2/N_2 compared to ambient air, the other slightly low. Replicates of flasks collected on a given date and time are then divided so that some flasks are analyzed against the high and others against the low working tank. If the factor of 1.14 is in error, this will yield systematic offsets between the two types of flasks. Analyses which allow verification of the 1.14 factor on a continuous basis are shown in Figure 11, which indicate that the factor of 1.14 has remained stable to better than 2% over the period from 2002 to present. The factor was unchanged despite a new analysis procedure that was adopted in 2007, when the pressure in the analysis line, upstream of the flask, was adjusted to match each flask individually, thus minimizing pressure changes during flask sweep-out.

Uncertainty in the flask sweep-out correction is more relevant for some features in the O_2/N_2 records than others. The long-term atmospheric O_2/N_2 trend measured by flasks, for example, is relatively insensitive to the sweep-out correction which scales with the difference in O_2/N_2 between flasks and working tanks. Individual working tanks typically last ~ 8 months, with the new tanks being filled from near-background ambient air. Over the long-term, the working tank concentrations have trended downwards in parallel with the atmospheric data, as shown in Figure 12. The observed long-term trend is therefore mostly controlled by tank-to-tank (i.e. working-tank to long-term reference gas differences) rather than by flask-to-tank differences. We estimate that uncertainty in the flask sweep-out correction can contribute errors in the long-term O_2/N_2 trend of at most 0.5%, with the percentage decreasing as the records grows in length. The seasonal cycles are potentially more sensitive, because the working tanks

do not track the cycles at individual stations. We estimate, for example, that the uncertainty in the sweep-out correction can cause errors in measured seasonal amplitudes in O_2/N_2 of at most 1 to 2%.

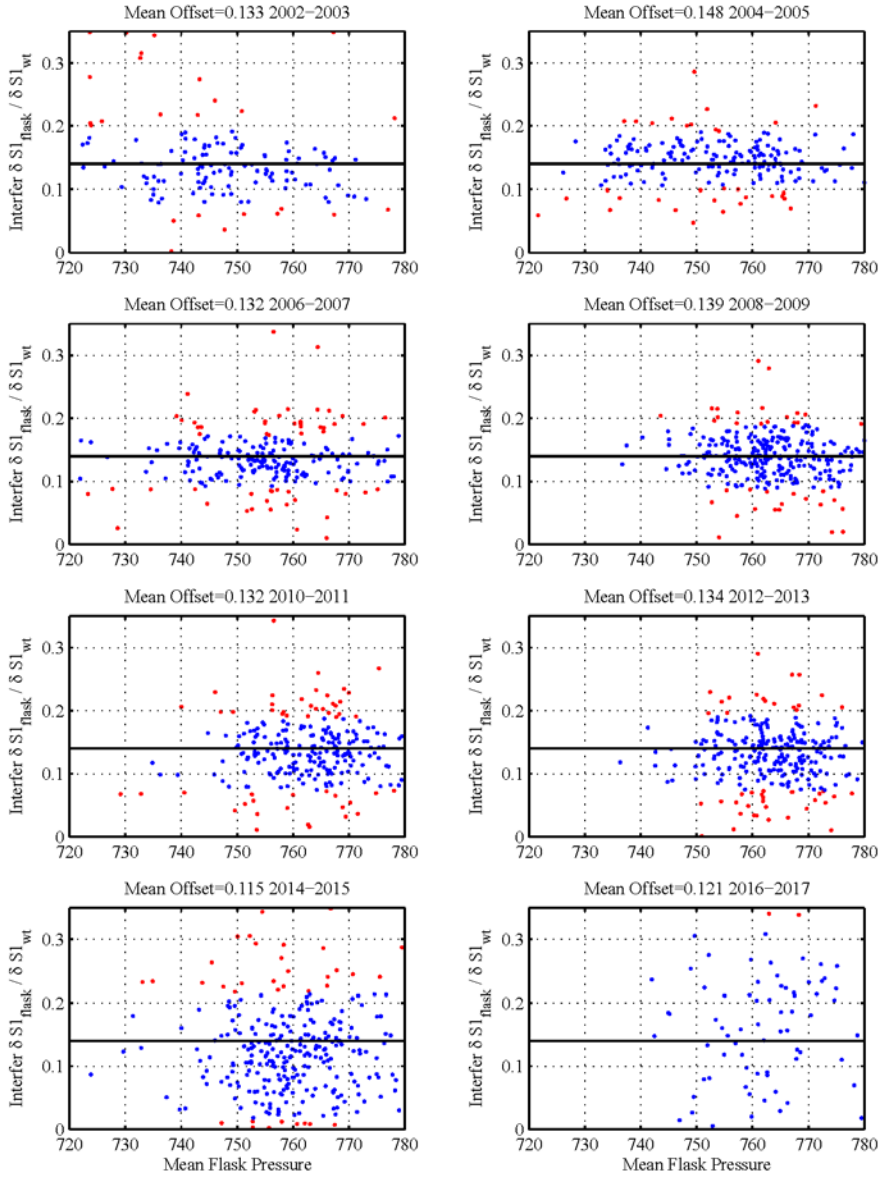

Figure 11. Flask sweep-out calibration cross checks. The y axis of each plot is the mean offset for flask replicates analyzed against the high versus low working tanks on a given analysis date. The offset is expressed as a fraction of difference between the high and low working tanks. A value of 0.14, for example, means that that peaks measured against the high tank are offset from the peaks measured against the low working tank by 14% of the difference between the tanks. Offsets here are measured in "refractivity" units, closely related to O_2/N_2 ratios prior to the CO_2 interference correction applied. The workup has adopted a nominal value of 0.14 to correct for the offset, indicated by the black line. The mean offset, calculated from the flask replicates for each 2-year is indicated above each plot. The red points were excluded as outliers from this average calculation. The increased scatter after 2014 results

from using high and low working tanks that were closer in concentration, which reduced the precision in resolving the offsets.

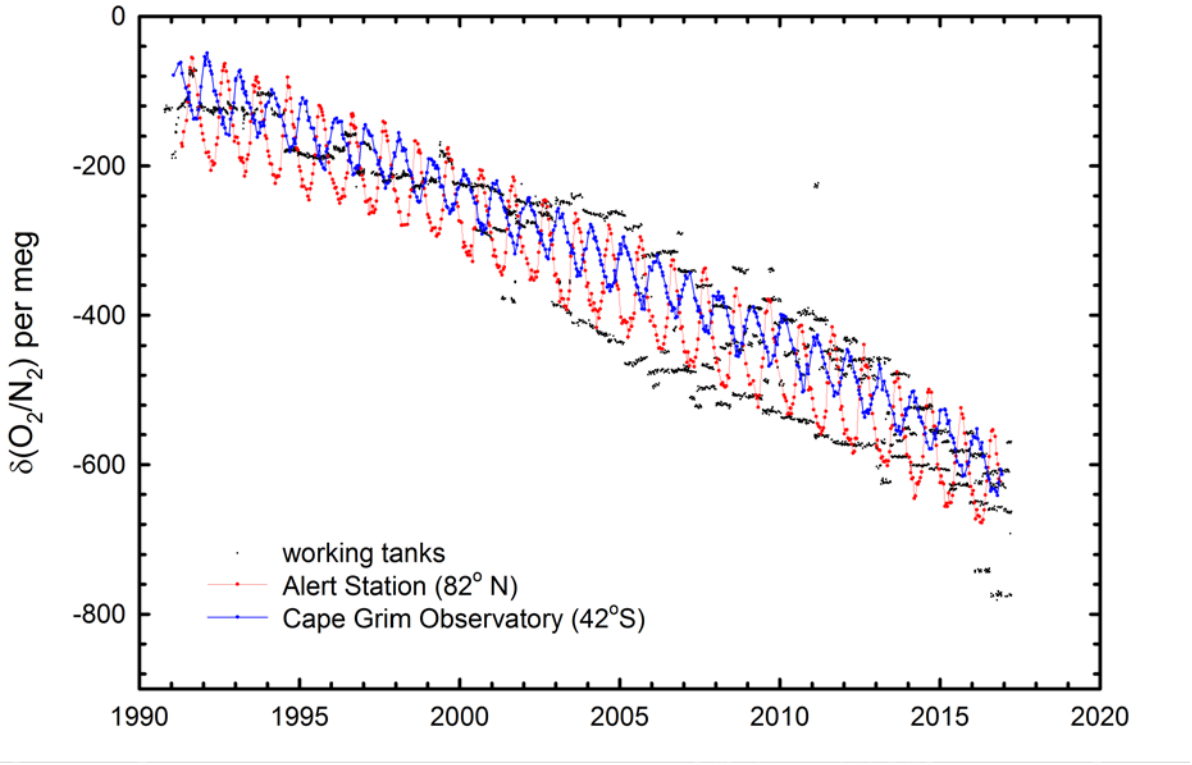

Figure 12. Working tank (small black points) versus time. Also shown are daily flask averages from flask replicates collected at Alert Station and Cape Grim Observatory. All data shown on same scale (S2 scale prior to scale change implement in this report).

7. Updating the O_2 database for the revised span sensitivity

This sections details methods used to update the O_2 database so it is fully consistent with the revised span sensitivity parameters detailed in Section 3.

Data reduction for the interferometric O_2/N_2 measurements was originally implemented in the Paradox database environment that was migrated to Microsoft Access in 1999 since Paradox did not have a fix for the Y2K bug. In these Paradox and Access environments, parameters from each flask analysis date (e.g. cylinder or flask ID numbers, laboratory conditions, jog values) were manually entered into input tables within Paradox or Access. A

series of “queries” were used to calculate intermediate parameters such as instrument span as well as final concentrations that then populated output tables in the database.

In the early 2000s, coding changes were made to replace the Access workup with code written in the *matlab* environment that allowed the jogs values to be determined directly from the raw digital data. This reduced the need for manual data entry and provided a more flexible and transparent coding environment for the algorithms. The data flow in the *matlab* environment closely matched the data flow in Access environment, with identical formulas, etc. The *matlab* environment was applied uniformly to all analyses after Feb. 2001, while the Access environment was continued through September 2004, allowing comparison between the *matlab* and Access from February 2001 to September 2004. With the update, the Access-driven data reduction path retained the manually-entered Access data files, but used the *matlab* scripts for further data reduction. A date in July 2003 was adopted for transitioning from one approach to the other in the main workup. The pre- and post-2003 data reduction paths both needed to be updated to incorporate the new span sensitivities.

Unless otherwise indicated, the methods described below apply to pre-2003 workup path. Any significant differences for the post-2003 workup are described where necessary.

Prior to this span update, the O_2/N_2 data was worked up using the span formula:

$$O2span = 6.04*(2537/4360) /((P - P_0)*P_{cal}*3.324\times10^{-8})\times10^4) \quad (21)$$

where *O2span* is in units of per meg per ten thousandths of a fringe. This formula is derivable from Eq (17) and (18). In practice Eq. (21) was applied with a constant value of $P_{cal} = 2210$.

With this update, we implement the new span formulas based on Eq. (18) and (19):

$$OPD_{samp} = (P - P_0)*P_{calnorm} /((T_{lab} + T_{cor} + 273.15)/294.15) \quad (22)$$

$$O2span = 1/((.209436)(1-.209436))*(2537.2688/4359.5662)/(3.3966\times10^{-8}\times OPD_{samp}\times10^4) \quad (23)$$

The method for propagating the Scripps O_2/N_2 scale based on tank comparisons is described in Keeling et al. (1998). The zero of the Scripps $\delta(O_2/N_2)$ per meg scale was based on the composition of air delivered from cylinder HA7017 in Oct. 1990. At that time, tank HA7017 was compared against two reference tanks that served as high and low spans for CO_2 (but not O_2/N_2) and hence are called high-span and low-span tanks. These span tanks were then used to calibrate working tanks and flask determinations. As the initial high and low-spans were consumed, they were then analyzed against replacement high- and low-spans, etc., with the system propagating forward in time, replacing high- and low-span tanks as they became

depleted. For the purpose of initial data workup, all the high- and low-spans were assumed to have time invariant concentrations based on initial assignments. This initial workup is known as the S1 scale. Further corrections were then applied for slow drift in this initial S1 scale based on measurements of long-term reference tanks. This corrected scale is known as the S2 scale. The S1 to S2 corrections were subject to retrospective revision based on the evolving insight into S2 scale drift provided by the long-term reference tanks. The S1 values are not changed during this updating.

In strategizing for how to update the scale for the new span coefficients implemented with this report, it was decided to rework the full dataset from the onset in 1990, thus also recalculating values for all the high- and low-spans and thereby changing the S1 values. An alternative would have been to apply the update via an appropriate revision of the S1 to S2 corrections. Although the adopted approach required extensive recalculations, it had the advantage of avoiding the need for using two versions of the span coefficients (old and new) at different stages in the workup.

Recalculating S1 cylinder values

With a few exceptions that are described below, the database was updated to account for the revised span coefficients as follows:

The interferometer span is calculated from the Eqs. (16), (18) and (19), using parameter values for *Psamp*, P_0 and *Tlab*, taken from the Access "highlow" table. These parameters are now stored in an input file named *labcond.csv*, and data from this file are used in the *matlab* workup. Values for $P_{calnorm}$ and T_{cor} covering 7 distinct time periods after 1989 (Table 3) are stored in a lookup table called *pcal.csv* . Plots of *PSamp, P0* and *Tlab* were shown previously in Figure 7.

The working tank concentrations in refractive index units, *CW*, are calculated as:

$$CW = (CHDec + CLDec - (HSFringe + LSFringe)*O2Span)/2 \qquad (24)$$

where *CHDec* and *CLDec* are the declared values of the high- and low-span tanks, also in refractivity unit and *HSFringe* and *LSFringe* are the fringe remainders in the comparison of the working tank with the high and low-span tanks.

These working tank concentrations and interferometer span values are then written to an output file *labdata_cor.csv* for later use in flask calculations. This output file mirrors the original MS Access output table "labdata".

Concentration of other cylinders, also in refractivity units, are computed according to

$$O2r = CW + JOG*O2Span \qquad (25)$$

where *JOG* is the fringe remainder differences from the working tank, *CW* and *O2Span* are taken from the *labdata_cor.csv*, using entries from dates that are indicated in the others table. Data from these analyses are stored in the "others" Access table.

For the pre-2003 workup, the O_2/N_2 readings on the S1 scale were previously calculated according to:

$$O2S1 = O2r - (CO2S1 - 363.29)*1.1156 \quad (26)$$

where *CO2S1* is the concentration of CO2 in the gas as measured on the Siemens analyzer's linear S1 calibration scale. The CO2 S1 scale differs from the true CO2 mole fraction on the S2 scale by a non-linear quantity that varies from roughly 0.2 ppm at 360 ppm to 2.6 ppm at 410 ppm. In the early 1990s when background air was around 360 ppm, the difference between the CO2 S1 and S2 scales was small enough to be ignored. In Sept 2007, the *matlab* workup was updated to incorporate CO2S2 instead of CO2S1 values in Eq. (26), but this 2007 update was applied only to the post-2003 *matlab* workup. As part of the current update, we therefore also have changed the algorithm to use S2 values before 2003, using the following formula for both pre- and post-2003 workups:

$$O2S1 = O2r - (CO2S2 - 363.29)*1.0919 \quad (27)$$

where the CO_2 interference factor (Table 2) has also been updated to reflect the span change.

Corrected concentrations for all "other" cylinder are written in an output file *others_cor.csv* that mirrors the original MS Access output table "*others*".

Reassigning the first high-span and low-span pair

Previously, the assigned values for the first high- and low-span tanks, 635863 and 635865, were − 64.80 and −138.30 per meg, respectively. Because these initial assignments were based on a single comparison in Oct. 1990 to tank HA7017 (see page 36 of lab notebook 7), the anchoring of the scale to tank HA7017 was not very precise. Although this imprecision was of little relevance for subsequent atmospheric trends (which were ultimately tied to a scale anchored to a suite of long-term reference gases), the imprecision is nevertheless important for comparison with measurements made at Scripps in 1989, which were also based on HA7017. Recognizing this issue, we have revisited here the anchoring of the scale to HA7017.

We thus examined a suite of runs on tank HA7017 over the period from late 1990 to mid 1992. The mid-1992 end date was selected because HA7017 was thereafter run in a horizontal orientation in the "Blue Box" which shifted upwards the O_2/N_2 ratio delivered from this tank (Keeling et al., 1998). We then developed an iterative procedure to adjust the per-meg values for the first high- and low-span pair (635863 and 635865) so that the average of all these measurements for HA7017 equaled 0 per meg. This adjustment involved increasing the declared

values on 635863 and 635865 upwards by 4.91 per meg, to yield new declared values of -133.39 and -159.89 per meg compared to previously declared values of -138.30 and -164.80 per meg. In the adjustment, we fixed the difference between 635863 and 635865, thus neglecting a ~ 2 % scale contraction in their difference, which was too small to be of importance.

The 9 measured values for HA7017 calculated in this manner after adjustment of the high- and low-span tanks are shown in Figure 13.

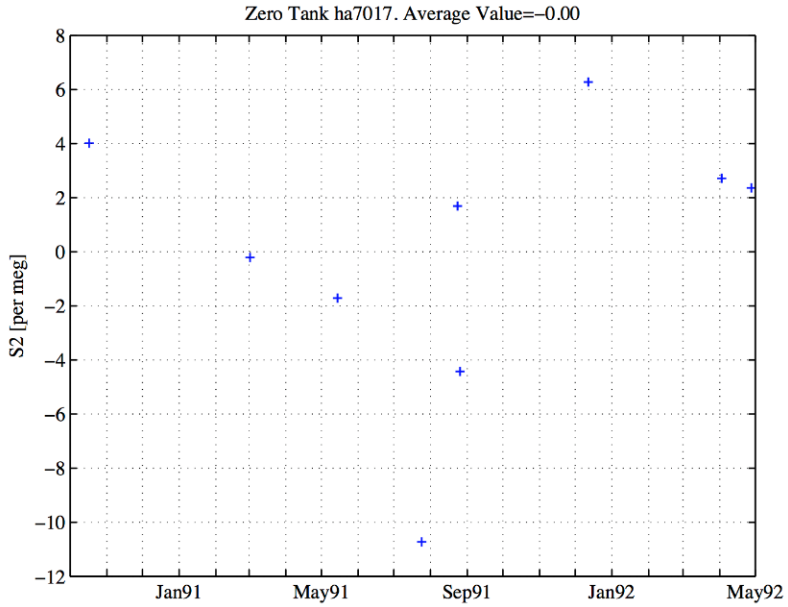

Figure 13. Concentration of the original zero calibration cylinder HA7017 measured against the first hi-span and lo-span calibration cylinders. Values were calculated using corrected interferometer span value and declarations for the hi/lo pair were increased by 4.91 per meg.

Reassigning subsequent high- and low-spans

Replacement high- and low-span tanks go through a grooming period during which they are run as “other” cylinders against the previous high- and low-span tanks. The next high- and low-span tanks are assigned values based upon an average of a select group of these early overlapped runs. From examination of old lab books we were able to identify individual runs of each next high and low-span run that were used previously in the assignment, and these were labeled with a “Y” in a new field called “UseO2” that was added to the “others” table. It was then possible to assign new declared values by calculating averages of individual runs tagged in the others table. A list of all the high- and low-span span tanks with old and corrected declared values is shown in Table 10:

Table 10: Corrected values for all hi-span and lo-span tanks all on refractivity-based scale.

Cylinder ID	First Use	Corrected O2 per meg	Original O2 per meg	Corrected /Original	Corrected-Original
635865-19890101	1990-10-16	-133.39	-138.30	0.9645	4.910
635863-19890101	1990-10-16	-159.89	-164.80	0.9702	4.910
465062-19890101	1991-03-23	-135.46	-140.60	0.9634	5.144
?????-19920324	1992-04-30	-143.59	-148.63	0.9661	5.036
nd01530-19911021	1994-01-15	-141.94	-147.01	0.9655	5.067
nd02701-19950110	1995-05-05	-186.39	-192.04	0.9706	5.655
nd02702-19950714	1995-10-10	-225.98	-232.02	0.9740	6.035
nd01530-19960119	1997-03-13	-206.31	-212.15	0.9725	5.838
nd02707-19960314	1997-05-13	-219.91	-225.88	0.9736	5.971
nd06875-19960314	1998-05-22	-237.41	-243.64	0.9744	6.234
nd02702-19970815	1998-07-15	-210.60	-216.23	0.9739	5.633
nd10340-19980406	1999-05-18	-217.02	-223.00	0.9732	5.977
nd06870-19980406	1999-08-17	-267.16	-273.84	0.9756	6.681
nd01530-19990305	2000-08-23	-209.38	-215.24	0.9728	5.861
nd10276-20000101	2001-02-01	-201.01	-206.74	0.9723	5.723
nd02709-20010510	2002-02-06	-262.44	-269.33	0.9744	6.886
nd02728-19990915	2002-09-12	-229.23	-235.49	0.9734	6.262
nd16636-20020430	2004-05-06	-346.70	-354.75	0.9773	8.046

Reassigning flask concentrations

Raw data recorded during flask analyses are stored in the Access table named “chart”. This includes the flask ID, a measure of the fringe remainder difference between flask and working tank based on strip-chart recorded divisions (*O2Div*), a measure of the change in flow during analysis, used in the flask pressure calculation (*FR*), and the chart scale factor (*O2ChartSc*) to convert chart divisions to ten thousandths of a fringe. These data, combined with the corrected working tank and span values that were previously saved in the file *labdata_cor.csv* described above allow recalculation of the flask oxygen concentrations. The calculation proceeds as follows.

O2Prelim is calculated as

$$O2Prelim = O2Div*O2ChartSc*O2Span + O2WT \quad (28)$$

A correction for the jog sweepout is calculated as

$$O2Cor = O2Div*O2ChartSC*O2Span*O2Sweep \quad (29)$$

where the sweep-out correction is determined from flask pressure *Press* as

$$O2Sweep = 1/(2.769 + Press*(-0.00575 + 0.0000042*Press)) - 1 \quad (30)$$

and flask pressure is determined from a measure of the flow deviation (*FR, for "flow ratio"*) when measuring a flask:,

$$Press = 818.6 + FR*(-8.22 - 51.5*FR) \quad (31)$$

The flask sweep-out correction and the CO_2 interference correction are then applied in a single step to obtain S1 values:

$$O2S1 = O2Prelim + O2Cor - (CO2S2 - 363.29)*1.0919 \quad (32)$$

where *O2Prelim* and *O2Cor* are taken unchanged from the results table.

Corrected flask concentrations are written in an output file *results_cor.csv* that mirrors the original MS Access flask output table "*results*".

Eqs. (28) to (32) apply to the early Access workup method, where flask peaks were ruled by hand on the strip chart. In the later *matlab* workup, the method was changed to being based on fitting sweep-out templates (see Section 6) which replaced equations (28), (29), (30), and (31) with this single fitting step.

Rework of 1989 flask data

As mentioned above, the database also includes flasks sampled from the end of the Scripps Pier in 1989 that were also analyzed in 1989, while the interferometer was at Scripps and before the high- and low-span calibration procedure had been implemented. These early runs were conducted under different laboratory conditions, with a sample cell pressure of about 2150 torr compared to ~1800 torr used later at NCAR. These flasks were run against working

tanks that had been directly compared to tank HA7017, rather than indirectly compared via high- and low-span tanks.

These analyses were previously worked up using values for interferometer span, working tanks and jog sweepout that were calculated outside of the Access database and these values were hardwired in the "*labdata*" table. The hard-wired values were set for 3 analysis dates in 1989. In examining this previous workup (see Appendix C), it was discovered that the original refractivity ratio sensitivity of $S_{O2} = 3.1\times10^{-8}$ was used, rather than the value of $S_{O2} = 3.324\times10^{-8}$ which was used for all other workup after Aug. 1993 (see Table 2). The previous span update in Aug. 1993 evidently failed to include updating the span for these early La Jolla data. The corrections for these data to bring them to the modern scale is therefore somewhat larger than for the data after Aug 1993.

To update these data, we take account of the span change impact on both the declared values of the working tanks, as well as in the differences between the flasks and the working tanks.

For the working tank declarations, we scaled the earlier values by the factor of 0.91417, so that $WT_{new}=0.91417*WT_{old}$. This factor includes correction to the refractivity ratio sensitivity to O_2 from 3.1×10^{-8} to 3.3966×10^{-8}, as well as additional corrections for more precise estimates of the Hg lamp wavelengths, the absolute O_2 mole fraction in tank HA7017, and new estimates for P_{cal}. The additional changes modify the correction factor from 0.91267 to 0.91417, a change of only ~0.16%. The working tank determinations are detailed in Table 11. We could not locate the exact calculations supporting the original working tank declarations, but we verified that they were reasonably concordant with values tabulated in Lab Notebook #7, pages 10 and 11.

Table 11. Declared values for working tanks used in 1989

Tank	*Original value in Access database*	*Recalculation of original values based on tables in Lab Notebook #7 pages 10 and 11, by tank analysis date in 1989*[*]				*New WT declaration, after rescaling*
		14 March	5 April	13-14 June	13 Sept.	
465060	−143.2887	−149.07	−145.62	−143.33	−145.26	−130.99
635869	−160.0147			−161.27	−158.85	−146.28
64284	+17.2695				+17.27	+15.79

[*]Entries from Notebook #7 in "ppm" were multiplied by a factor of 6.04 to convert to per meg

For the flask working-tank differences, we used parameters detailed in Table 12. The interferometer span and working tank values calculated in this way have been written to the

corrected labdata output file, "*labdata_cor.csv*". The flask jog sweepout correction was previously given a fixed value of *O2Sweep*=0.16 rather than being calculated from the flask pressure, and this value was retained in these calculations. Corrected flask values for the 1989 analyses are included in the updated results output file, "*results_cor.csv*".

Table 12. Parameters used in the span calculation for 3 dates in 1989. Derived interferometer span value is shown in the last column

Flask analysis Date	*PSamp*	*TLab*	*PZero*	P_{cal}	*O2Span*
23-May-1989	2097	21.1	0.0	2205.7	2.238171
07-Jul-1989	2131	21.1	0.0	2205.7	2.202461
16-Sep-1989	2174	21.1	0.0	2205.7	2.158898

S1 to S2 corrections

No changes were made here to the S1 to S2 corrections as part of this revised workup. The S1 to S2 corrections are at the level of ~7 per meg or smaller, and a span change of 2% would have changed these by only 0.15 per meg, which we neglect.

Appendix A. Sensitivity of the refractivity ratio to N_2 versus O_2

Eq. (7) provides a suitable formula for estimating $\delta(O_2/N_2)$ from measurements of refractivity ratio after applying interference corrections. For an addition of N_2 to an air sample, this leads to changes in all terms on the right hand side of Eq. (7), including the interference terms, via changes in $\delta(Ar/N_2)$ and the trace gases (via dilution). An alternate perspective on these interferences is to consider the relative sensitivity of the refractivity ratio to O_2 versus N_2.

We define the relative sensitivity to N_2 versus O_2, as the amount of N_2 that must be added to a sample to produce in a measured quantity of the same magnitude (but opposite sign) as a unit addition of O_2. This relative sensitivity can be calculated for several possible measured quantities:

O_2/N_2 ratio:

$$\text{Relative sensitivity} = X_{O2}/X_{N2}$$

$$= 0.209448 /0.78082 = 0.26824$$

O_2 mole fraction:

$$\text{Relative sensitivity} = X_{O2}/(1-X_{O2})$$

$$= 0.209448/(1-0.209448) = 0.26494$$

Relative refractivity:

$$\text{Relative sensitivity} = S_{N2}\,(1-X_{N2})/(S_{O2}(1-X_{O2}))$$

$$= 3.2479(1-0.78084)/(3.3973(1-0.209448)) = 0.26503$$

O_2/N_2 ratio calculated from relative refractivity after Ar/N_2 correction:

$$\text{Relative sensitivity} = 0.26503 - (I_{Ar/N2})(X_{O2}/X_{N2})$$

$$= 0.26503 - (-0.0124)(0.209448/0.78082) = 0.26836$$

The inputs to these calculations are from Table 1. These calculations show that the relative refractivity is 1.20% less sensitive to N_2 addition (relative to O_2) than the O_2/N_2 ratio. This is very similar to a measurement of O_2 mole fraction, which is 1.23% less sensitive. The last calculation shows that applying the Ar/N_2 correction reduces the difference to 0.04%. This remaining offset is due to dilution effects on trace gases, and could be reduced by applying interference corrections for the small change in trace-gas corrections.

Appendix B. Fringe remainder sensitivity to absolute refractivity

As noted in Section 2, the fringe remainder is sensitive, in principle, both to changes in refractivity ratio and absolute refractivity of the sample. To quantify the impact of absolute refractivity changes, we start by differentiating Eq. (12), now allowing that $\tilde{r}_{samp}$ and $OPD_{samp}(\lambda_2)$ both depend on the O_2 mole fraction in air:

$$\frac{d\varepsilon_1}{dX_{O2}} = \frac{\lambda_2}{\lambda_1} OPD_{samp}(\lambda_2) \cdot \left[S_{O2} + (\tilde{r}_{samp} - \tilde{r}_{scan}) \frac{1}{r_{samp}(\lambda_2)} \frac{dr_{samp}(\lambda_2)}{dX_{O2}} \right] \tag{A1}$$

where $r_{samp} = n_{samp} - 1$ is the absolute refractivity, and where we have used Eq. (2) as well as the relation

$$\frac{1}{OPD(\lambda_2)} \frac{dOPD(\lambda_2)}{dX_{O2}} = \frac{1}{r_{samp}} \frac{dr_{samp}(\lambda_2)}{dX_{O2}} \tag{A2}$$

The second term in the bracket in Eq. (A1) is the additional contribution from changes in absolute refractivity, which appears as an additive correction to the refractivity ratio sensitivity coefficient S_{O2}. This term was neglected in Eq. (16).

If the sample is essentially normal air, it is easily shown that

$$\frac{1}{r_{samp}(\lambda_2)} \cdot \frac{dr_{samp}(\lambda_2)}{dX_{O2}} = \frac{1}{r_{air}(\lambda_2)} \cdot \frac{r_{O2}(\lambda_2) - r_{air}(\lambda_2)}{1 - X_{O2}} \tag{A3}$$

which is a sensitivity factor for the absolute refractivity (at a single wavelength) to changes in O_2 mole fraction and can be shown, using constants in Table 1, to have a value of -8.8×10^{-8} ppm^{-1} at $\lambda_2 = 4360$ Å.

The relevant term in Eq. (A1) also contains the factor of $\tilde{r}_{samp} - \tilde{r}_{scan}$. To quantify this factor, we note that sample gases and scan gases are always normal air with very similar composition, but at different pressures (and densities). Taking a typical sample gas pressure of ~1750 torr and a scan gas pressure < 20 torr, and density sensitivity as determined in Keeling (1988, Appendix B), yields $\tilde{r}_{samp} - \tilde{r}_{scan} \sim 2.0 \times 10^{-5}$.

Multiplying these two factors yields $(-8.8 \times 10^{-8}\ \text{ppm}^{-1})(2.0 \times 10^{-5}) = -1.8 \times 10^{-12}\ \text{ppm}^{-1}$, which is more than 10^4 times smaller than $S_{O2} = 3.4 \times 10^{-8}\ \text{ppm}^{-1}$. The contribution to changes in the fringe remainder arising from changes in absolute refractivity is thus negligible.

Appendix C. Email from Ralph Keeling, January 2017

From: Keeling, Ralph

Sent: Monday, January 30, 2017 1:55 PM

To: 'Stephen Walker' <sjwalker@ucsd.edu>

Subject: RE: results database

Stephen,

Notes from today's meeting:

As we verified, the access database handled the 1989 flask analyses with hardwired values of the O2 span and working tanks, rather than values calculated from Psamp, Pzero, etc.

I verified that these hard-wired spans, both for working tanks and flasks were generated using the original SO2 refractivity ratio sensitivity of 3.10e-8. This was an oversight, because there should have been an update to a value of 3.324e-8 starting in 1993, when the rest of the workup was changed to use this newer value. For the working tanks, I pulled numbers from the original Lab Notebook 7 pages 10 and 11, which gave numbers for tank offsets in "ppm O2 equivalent" and showed that, by multiplying these by 6.04 = 1/.20946/(1-0.20946), I could reproduce the hardwired values to within ~1% (see next worksheet). The numbers in the notebooks were generated with the formula:

O2span = 6.04/((Psamp-Pzero)*2.21*3.10e-8)*(2537/4360)*1e-4

I also verified that this formula reproduced the hard-wired O2 span that was used from the flask workup based on values for Psamp and Pzero that were found in the old notebooks for the 1989 analysis dates.

Although it doesn't require any special attention, it is notable that the value of Psamp used in 1989 was around 2150 torr, i.e. quite a bit higher than values of around 1800 torr used at NCAR and subsequently. The change presumably reflects the need to run the Siemens analyzer at the lower ambient barometric pressure that prevails at NCAR.

To implement the updated span for the 1989 analyses, we can use the same algorithms as for later flasks. This calculation uses these inputs, which are also detailed on the attached worksheet:

Psamp:

Pzero:

Pcal,norm: 2205.7 fringes per torr - use this same number for all three 1989 analysis dates

Tlab: 21.1C - use this number for all three 1989 analysis dates

DeltaT: 0 - use this zero value for all three 1989 analysis dates 273.15, 294.5 - these are fixed constants in our formula, same values as before.

For the post 1989 analyses, I think you already have a lookup-table for Pcal,norm, Tlab, and DeltaT, so it should just be a matter of adding one more row to this table, if it isn't there already. The Psamp and Pzero, from the notebooks, are on the attached.

For reassigning the 1989 working tanks, I suggest scaling the old assignments as follows:

New assignment = (old assignment)*0.91417

The factor of 0.91417 is justified on the attached spreadsheet. It is very nearly equal to the ratio of 3.1/3.3966 of the change in So2 (i.e. the refractivity ratio sensitivity to O2) but I also folded in small difference associated with more precise estimates of the Hg lamp wavelengths, the absolute O2 mole fraction in tank 7017, and a new estimates for the Pcal (fringe/torr from countup). The impact of these is to change the scale factor by ~0.16%.

We also verified that the sweepout correction was hardwired to upscale the O2 peaks in these early flasks by a factor of 1.16, as detailed on Labbook #6, page 117.

-Ralph

References

Aoki, N., S. Ishidoya, N. Matsumoto, T. Watanabe, T. Shimosaka and S. Murayama (2019). "Preparation of primary standard mixtures for atmospheric oxygen measurements with less than 1 μmol mol−1 uncertainty for oxygen molar fractions." Atmospheric Measurement Techniques **12**(5): 2631-2646.

Blaine, T., W. (2005). Continuous Measurements of Atmospheric Ar/N_2 as a Tracer of Air-Sea Heat Flux: Models, Methods, and Data, University of California, San Diego.

Cuthbertson, C. and M. Cuthbertson (1910). "On the refraction and dispersion of air, oxygen, nitrogen, and hydrogen, and their relations." Proceedings of the Royal Society of London. Series A, Containing Papers of a Mathematical and Physical Character **83**(561): 151-171.

de Laeter, J. R., J. K. Böhlke, P. De Bièvre, H. Hidaka, H. Peiser, K. Rosman and P. Taylor (2003). "Atomic weights of the elements. Review 2000 (IUPAC Technical Report)." Pure and applied chemistry **75**(6): 683-800.

Edlén, B. (1966). "The refractive index of air." Metrologia **2**(2): 71.

Glueckauf, E. (1951). The composition of atmospheric air. Compendium of Meteorology. T. Malone. Boston, American Meteorological Society**:** 3-10.

Kaufman, V. (1962). "Wavelengths, energy levels, and pressure shifts in mercury 198." Journal of the Optical Society of America **52**(8): 866-870.

Keeling, R. F. (1988a). Development of an interferometric oxygen analyzer for precise measurement of the atmospheric O_2 mole fraction, Harvard University.

Keeling, R. F. (1988b). "Measuring correlations between atmospheric oxygen and carbon-dioxide mole fractions - a preliminary-study in urban air." Journal of Atmospheric Chemistry **7**(2): 153-176.

Keeling, R. F., P. Guenther, S. Walker and D. Moss (2016). Scripps Reference Gas Calibration System for Carbon Dioxide-in-Nitrogen and Carbon Dioxide-in-Air Standards: Revision of 2012. La Jolla, California, Scripps Institution of Oceanography**:** 1-173.

Keeling, R. F. and A. C. Manning (2014). Studies of recent changes in atmospheric O_2 content. Treatise on Geochemistry, Volume 5. R. F. Keeling and L. Russell. Amsterdam, Elsevier**:** 385-404.

Keeling, R. F., A. C. Manning, E. M. McEvoy and S. R. Shertz (1998). "Methods for measuring changes in atmospheric O_2 concentration and their application in southern hemisphere air." Journal of Geophysical Research-Atmospheres **103**(D3): 3381-3397.

Keeling, R. F., A. C. Manning, W. J. Paplawsky and A. C. Cox (2007). "On the long-term stability of reference gases for atmospheric O_2/N_2 and CO_2 measurements." Tellus Series B-Chemical and Physical Meteorology **59**(1): 3-14.

Ladenburg, R. and G. Wolfsohn (1932). "Untersuchungen über die Dispersion von Gasen und Dämpfen und ihre Darstellung durch die Dispersionstheorie." Zeitschrift für Physik **79**(1-2): 42-61.

Machta, L. and E. Hughes (1970). "Atmospheric Oxygen in 1967 to 1970." Science **168**(3939): 1582-1584.

Manning, A. C. and R. F. Keeling (2006). "Global oceanic and land biotic carbon sinks from the Scripps atmospheric oxygen flask sampling network." Tellus **58B**: 95-116.

Resplandy, L., R. Keeling, Y. Eddebbar, M. Brooks, R. Wang, L. Bopp, M. Long, J. Dunne, W. Koeve and A. Oschlies (2019). "Quantification of ocean heat uptake from changes in atmospheric O_2 and CO_2 composition." Scientific Reports **9**(1): 1-10.

Severinghaus, J. P. (1995). Studies of the terrestrial O_2 and carbon cycles in sand dune gases and in Biosphere 2, Columbia University.

Stoll, E. (1922). "Die Dispersion der Luft und ihrer Hauptbestandteile im Spektralintervall: 4388–9224 Å.-E." Annalen der Physik **374**(18): 81-111.

Svensson, K.-F. (1960). "Measurements of the dispersion of air for wavelengths from 2302 to 6907 A." Arkiv for Fysik **16**(4): 361-384.